

ADDITIVE MANUFACTURING AND CHARACTERIZATION OF METAL
PARTICLE INCORPORATED POLYMER MATRIX FUNCTIONALLY
ENHANCED COMPOSITES

A THESIS SUBMITTED TO
THE GRADUATE SCHOOL OF NATURAL AND APPLIED SCIENCES
OF
MIDDLE EAST TECHNICAL UNIVERSITY

BY

ÖZGÜR UYAR

IN PARTIAL FULFILLMENT OF THE REQUIREMENTS
FOR
THE DEGREE OF MASTER OF SCIENCE
IN
METALLURGICAL AND MATERIALS ENGINEERING

DECEMBER 2023

Approval of the thesis:

**ADDITIVE MANUFACTURING AND CHARACTERIZATION OF METAL
PARTICLE INCORPORATED POLYMER MATRIX FUNCTIONALLY
ENHANCED COMPOSITES**

Submitted by **ÖZGÜR UYAR** in partial fulfillment of the requirements for the degree of **Master of Science in Metallurgical and Materials Engineering, Middle East Technical University** by,

Prof. Dr. Halil Kalıpçılar
Dean, Graduate School of **Natural and Applied Sciences** _____

Prof. Dr. Ali Kalkanlı
Head of the Department, **Metallurgical and Material Eng.** _____

Prof. Dr. Arcan F. Dericioğlu
Supervisor, **Metallurgical and Material Eng.** _____

Examining Committee Members:

Prof. Dr. Cevdet Kaynak
Metallurgical and Materials Eng., METU _____

Prof. Dr. Arcan F. Dericioğlu
Supervisor, **Metallurgical and Material Eng** _____

Prof. Dr. Ziya Esen
Mechanical Eng., Çankaya University _____

Assoc. Prof. Dr. Emre Büküşoğlu
Chemical Eng., METU _____

Assist Prof. Dr. Irmak Sargın
Metallurgical and Materials Eng., METU _____

Date: 04.12.2023

I hereby declare that all information in this document has been obtained and presented in accordance with academic rules and ethical conduct. I also declare that, as required by these rules and conduct, I have fully cited and referenced all material and results that are not original to this work.

Name Last name : Özgür Uyar

Signature :

ABSTRACT

ADDITIVE MANUFACTURING AND CHARACTERIZATION OF METAL PARTICLE INCORPORATED POLYMER MATRIX FUNCTIONALLY ENHANCED COMPOSITES

Uyar, Özgür

Master of Science, Metallurgical and Materials Engineering
Supervisor : Prof. Dr. Arcan F. Dericioğlu

December 2023, 75 pages

Increasing the structural capability of structures for various engineering applications while enhancing their functionality and reducing their weight by tailoring their internal morphology has always been a challenge for materials engineering. Advances in additive manufacturing (3D printing) methods have made it possible to tailor-design materials from micro to macro scale to fulfill these challenging property requirements. In this study, Fused Filament Fabrication (FFF) with metal powder incorporated polymer filaments has been used to process model structures with enhanced structural and functional capability. In this scope, the mechanical behavior of additively manufactured Triply Periodic Minimal Surface (TPMS) lattice structures such as Schwarz Primitive, IWP, and Neovius, which are commonly used lattice structures, has been investigated. FFF, being one of the most frequently used and feasible additive manufacturing techniques, was utilized to fabricate pristine polymer lattice structures with different relative densities of 30%, 40%, and 50% using Polylactic acid (PLA) and Polypropylene (PP) along with metal powder incorporated PP (metal/PP) composite lattice structures. The structural capability of the designed structures was determined by mechanically testing the additively

manufactured polymeric structures. Moreover, finite element analyses have also been conducted, and their results were compared with the results obtained experimentally. It has been demonstrated that for developing and optimizing metal particle containing filaments for various applications, including additively manufactured lattice structures, particle morphology, aspect ratio, and volume fraction along with even particle distribution and dispersion throughout the filament, significantly impact the processing quality and final properties of the 3D-printed structures.

It was generally concluded that incorporation of metal powder into PP (metal/PP) rendered it more processable for TPMS lattice structures compared to PLA (metal/PLA) filaments. However, despite the promising FEM results, the detachment issue in FFF printing hindered the ability of the composite filament with PP matrix (metal/PP) to meet the expected standards.

Compressive test results revealed significant insights. Pristine PLA exhibited higher compressive strength than PP in a fully dense cubic (bulk) form. Reinforcement enhanced the properties of the PP matrix proportionally with additive content. However, PLA matrix reinforcement did not uniformly improve mechanical properties, possibly due to air gaps trapped between the layers. Higher relative density boosted compressive strength in TPMS structures, with detachment issues more pronounced in PP models. Metal particle addition unevenly affected strength in the case of PP and PLA matrices. Pristine filament manufacturability surpasses composites, impacting cube and TPMS fabrication. Increasing relative density enhanced strength in lattice structures. Notably, the IWP model exhibited superior compressive yield strength attributed to its effective stress distribution and self-supported structure.

Keywords: Fused Filament Fabrication (FFF), Lattice Structure, Additively Manufactured Composites, Mechanical Testing, Relative Density

ÖZ

METAL PARÇACIK İLE BİRLEŞTİRİLMİŞ POLİMER MATRİS FONKSİYONEL OLARAK GÜÇLENDİRİLMİŞ KOMPOZİTLERİN KATMANLI İMALATI VE KARAKTERİZASYONU

Uyar, Özgür
Yüksek Lisans, Metalurji ve Malzeme Mühendisliği
Tez Yöneticisi: Prof. Dr. Arcan F. Dericioğlu

Aralık 2023, 75 sayfa

Çeşitli mühendislik uygulamaları için yapıların yapısal kapasitesini arttırırken, iç morfolojilerini düzenleyerek işlevselliklerini arttırmak ve ağırlıklarını azaltmak, malzeme mühendisliği için her zaman bir zorluk olmuştur. Katmanlı imalat (3D baskı) yöntemlerindeki ilerlemeler, bu zorlu özellik gerekliliklerini karşılamak için malzemelerin mikro ölçekten makro ölçeğe kadar özel olarak tasarlanmasını mümkün kılmıştır. Bu çalışmada, metal tozu içeren polimer filamentler içeren Erimiş Filament İmalatı (FFF), gelişmiş yapısal ve işlevsel kapasiteye sahip model yapıları işlemek için kullanılmıştır. Bu kapsamda yaygın olarak kullanılan kafes yapıları olan Schwarz Primitive, IWP ve Neovius gibi eklemeli olarak üretilmiş Üçlü Periyodik Minimal Yüzey (TPMS) kafes yapılarının mekanik davranışları incelenmiştir. En sık kullanılan ve uygulanabilir eklemeli üretim tekniklerinden biri olan FFF, Polilaktik asit (PLA) ve Polipropilen (PP) ile birlikte %30, %40 ve %50'lik farklı bağli yoğunluklara sahip saf polimer kafes yapılarını üretmek için kullanıldı. metal tozu içeren PP (metal/PP) kompozit kafes yapıları. Tasarlanan yapıların yapısal kapasitesi, eklemeli olarak üretilen polimerik yapıların mekanik olarak test edilmesiyle belirlendi. Ayrıca sonlu elemanlar analizleri de yapılmış ve sonuçları deneysel olarak elde edilen sonuçlarla karşılaştırılmıştır. Eklemeli olarak üretilmiş kafes yapıları, parçacık morfolojisi, en boy oranı ve hacim fraksiyonu dahil olmak üzere çeşitli uygulamalar için metal parçacık içeren filamentlerin geliştirilmesi ve optimize edilmesinin yanı sıra filament boyunca eşit parçacık dağılımı ve

dispersiyonun, işleme kalitesini ve nihai özellikleri önemli ölçüde etkilediği gösterilmiştir. 3D baskılı yapılardan.

Genel olarak metal tozunun PP (metal/PP) içerisine dahil edilmesinin, onu PLA (metal/PLA) filamentlerine kıyasla TPMS kafes yapıları için daha işlenebilir hale getirdiği sonucuna varılmıştır. Ancak umut verici FEM sonuçlarına rağmen FFF baskıdaki ayrılma sorunu, PP matrisli (metal/PP) kompozit filamentin beklenen standartları karşılama yeteneğini engelledi.

Sıkıştırma testi sonuçları önemli bilgiler ortaya çıkardı. Bozulmamış PLA, tamamen yoğun kübik formda PP'den daha yüksek basınç dayanımı sergiledi. Takviye, PP matrisinin özelliklerini katkı içeriğiyle orantılı olarak geliştirdi. Bununla birlikte, PLA matris takviyesi, muhtemelen katmanlar arasında sıkışan hava boşluklarından dolayı mekanik özellikleri eşit şekilde iyileştirmede. Daha yüksek bağıl yoğunluk, TPMS yapılarında basınç dayanımını artırırken, PP modellerinde ayrılma sorunları daha belirgindir. PP ve PLA matrislerinde metal parçacık ilavesi mukavemeti eşit olmayan bir şekilde etkiledi. Kusursuz filaman üretilebilirliği kompozitleri geride bırakarak küp ve TPMS imalatını etkiler. Göreceli yoğunluğun artırılması, kafes yapılarında mukavemeti arttırdı. Özellikle IWP modeli, etkili gerilim dağılımına ve kendi kendini destekleyen yapısına atfedilen üstün basınç akma dayanımı sergiledi.

Anahtar Kelimeler: Erimiş Filament Üretimi (FFF), Kafes Yapısı, Mekanik Test, Katmanlı İmalatla Üretilmiş Kompozitler, Bağıl Yoğunluk

To my father, Yüksel Uyar.

ACKNOWLEDGMENTS

I wish to thank my supervisor, Prof. Dr. Arcan F. Dericiođlu, for his invaluable guidance and unwavering support throughout my master's program. His profound expertise and continuous encouragement played a pivotal role in enabling me to successfully complete this research and compose this thesis.

I would also like to express my gratitude to Ömer Yaşan, Ertuđrul Büyükhergöl, Can Özaslangöz, Selin Cansu Gölboylu, Burak Sivri, Dođan Görkem Cansu as well as to Seren Özer and Dr. Seha Tirkeş for their invaluable technical assistance, which greatly contributed to the quality of this work.

Özgür Akçam and Özlem Karaman and GSI SLV-TR personal, I am deeply thankful for their flexibility and understanding during the research process, enabling me to navigate through the challenges with confidence.

Special appreciation goes to my dearest friend, Merve Atlıođlu, whose shared experiences and shared meals were a source of comfort and inspiration throughout the thesis journey. Her unwavering support during the toughest moments was a driving force behind the successful outcome.

I am grateful to my old friend İsmet for his munificence, patience during the thesis process, and motivating responses.

Once again, thank you all for being an integral part of this journey and for your significant contributions.

TABLE OF CONTENTS

ABSTRACT.....	v
ÖZ.....	vii
ACKNOWLEDGMENTS	x
TABLE OF CONTENTS.....	xi
LIST OF TABLES	xiv
LIST OF FIGURES	xv
CHAPTERS	
1 INTRODUCTION	1
2 LITERATURE REVIEW	3
2.1 Classification of Additive Manufacturing Techniques	3
2.1.1 Powder-Based Additive Manufacturing Techniques.....	4
2.2 Solid Based Additive Manufacturing Techniques	6
2.2.1 Liquid-Based Additive Manufacturing Techniques.....	6
2.3 Lattice Structures.....	17
2.3.1 Triply Periodic Minimum Surface (TPMS) Lattice.....	19
3 EXPERIMENTAL WORK.....	21
3.1 Starting Materials	23
3.1.1 Composite Filament Production	24
3.1.2 Production of the Cubic Specimens.....	28
3.1.3 Mechanical Characterization of Cubic Specimens by Compression Test.....	28

3.1.4	Producing of the TPMS Lattice Structures with FFF	28
3.1.5	Production of TPMS Lattice Structures with Pristine Polymeric Filaments	29
3.1.6	Production of TPMS Lattice Structures with Metal/Polymer Composite Filaments	31
3.2	Characterization Studies	32
3.2.1	Sample Preparation and Examination	32
3.2.2	Mechanical Characterization TPMS Lattice Structures by Compression Test	32
3.2.3	Calculation of Mechanical Properties with Rule of Mixture Method	34
3.2.4	Microstructural Characterization.....	36
3.2.5	Simulation of the Mechanical Behavior of TPMS Lattice Structures Through Finite Element Analysis.....	36
4	RESULT AND DISCUSSION	39
4.1	Microstructural Examination	39
4.1.1	Metal Powder.....	39
4.1.2	Composite Filament.....	40
4.2	Bulk Specimens Produced with FFF	42
4.2.1	Fully Dense Cubic Specimens.....	42
4.2.2	Compressive Test Results of Bulk Specimens	43
4.3	Lattice Structure Specimens Produced with FFF	44
4.3.1	TPMS Lattice Structure Specimens.....	44
4.3.2	Fracture Surface Analyses of Compression Tested TPMS Lattice Structures.....	47
4.3.3	Mechanical Properties of the TPMS Lattice Structures	51

4.4	Modeling of the Compression Behavior of the TPMS Lattice Structures	59
4.4.1	Compression Behavior Comparison between FEM and Experimental Test	62
5	CONCLUSION.....	67
	REFERENCES	71

LIST OF TABLES

TABLES

Table 3.1 Materials used for the production of TPMS.	23
Table 3.2 Composition and density of the filament produced by the first batch. ...	26
Table 3.3 Composition and density of the filament produced by the second batch.	26
Table 3.4 Composition and density of the filament produced by the third batch. ...	26
Table 3.5 FFF process parameters applied for the fabrication of TPMS lattice structures using pristine PLA and PP.....	30
Table 3.6 FFF process parameters applied for the fabrication of TPMS lattice structures using metal/polymer composite filaments.....	31
Table 3.7 Composition of Nital Reagent.	32
Table 3.8 Average cross section area for each TPMS used in compression tests...	34
Table 3.9 Volume fraction of composite filaments.	35
Table 3.10 Mechanical properties of the components.	35
Table 3.11 Basic properties of the 5 vol% Fe/PP composite from compression test and rule of mixture.....	37
Table 4.1 Compressive test results of the bulk specimens.....	44
Table 4.2 Compressive test results of TPMS lattice structures made of pristine PLA.	57
Table 4.3 Compressive test results of TPMS lattice structures made of pristine PP.	57
Table 4.4 Compressive test results of TPMS lattice structures made of 5 vol% Fe (/PLA) composite filaments.....	58
Table 4.5 Compressive test results of TPMS lattice structures made of 5 vol% Fe (/PP) composite filaments.....	58

LIST OF FIGURES

FIGURES

Figure 2.1 Classification of Additive Manufacturing Processes [1].	4
Figure 2.2 Typical SLM configuration schematic [4].	5
Figure 2.3 Lithography-based 3D print technologies: (left) SLA, (right) DLP [8].	7
Figure 2.4 Schematic representation of Fused Filament Fabrication methods [11].	9
Figure 2.5 Schematic representation of Fused Filament Fabrication Extruder [12].	10
Figure 2.6 Different reinforcement materials are utilized in composite filaments: (a) Particulate reinforcement, (b) short fiber reinforcement, and (c) continuous fiber reinforcement composites.	15
Figure 2.7 Classification of Cellular Solids [29].	18
Figure 2.8 TPMS-CMs with a 10% relative density, as shown in CAD drawings: (a) Primitive-CM, (b) IWP-CM, and (c) Neovius-CM, respectively. 3D-printed samples of the relative densities for (e) Primitive-CM (23.5%), (f) IWP-CM (25.6%), and (g) Neovius-CM (23.7%) [31].	20
Figure 3.1 Fully dense cubic specimen preparation steps.	21
Figure 3.2 TPMS specimen preparation steps.	22
Figure 3.3 Modelling of TPMS specimens with Finite Element Analysis.	22
Figure 3.4 Particle size distribution of the Fe powders used in this study.	24
Figure 3.5 Composite filament production set-up; (a) twin screw extruder setup, (b) composite granules, (c) charging granules to extruder, (d) and (e) filament winding.	27
Figure 3.6 3D CAD models of Schwarz Primitive, Neovius, and IWP TPMS lattice structures designed in this study.	29
Figure 3.7 FFF process by using (a) PLA and (b) PP filaments.	30
Figure 3.8 Minimum (a) and maximum (b) cross sectional area of Schwarz Primitive (30%).	34
Figure 4.1 SEM images of sieved Fe powders at (a) lower and (b) higher magnification.	39

Figure 4.2 SEM images of not sieved Fe powders at (a) lower and (b) higher magnification.	40
Figure 4.3 Cross sectional view of PP matrix composite filament with 30.8 vol% iron particles (a) horizontal and (b) vertical section.	41
Figure 4.4 Cross sectional view of PP matrix composite filament with 5 vol% iron particles (a) horizontal and (b) vertical section.	41
Figure 4.5 Cross sectional view of PLA matrix composite filament with 5 vol% iron particles (a) horizontal and (b) vertical section.	41
Figure 4.6 Printing surface of the bulk specimens made of PP matrix composite filaments filled with (a) 30.8 vol% and (b) 5 vol% iron particles.	42
Figure 4.7 3D-Printed TPMS lattice structures (a) PLA and (b) PP specimens with different relative densities.	45
Figure 4.8 Selected TPMS lattice structure specimens 3D printed using 5 vol% Fe/PLA composite filaments.	46
Figure 4.9 Selected TPMS lattice structure specimens 3D printed using 5 vol% Fe/PP composite filaments.	46
Figure 4.10 Fracture surfaces of TPMS lattice structures 3D printed using pristine PLA and compression tested at 15% strain (a, b) Schwarz Primitive, (c, d) Neovius and (e, f) IWP with 30% relative density.	48
Figure 4.11 Fracture surfaces of TPMS lattice structures 3D printed using pristine PP and compression tested at 15% strain (a, b) Schwarz Primitive, (c, d) Neovius and (e, f) IWP with 30% relative density.	49
Figure 4.12 Fracture surfaces of TPMS lattice structures 3D printed using 5 vol% Fe/PLA composite filaments compression tested at 15% strain (a) Schwarz Primitive, (b) Neovius, and (c) IWP.	50
Figure 4.13 Fracture surfaces of TPMS lattice structures 3D printed using 5 vol% Fe/PP composite filaments compression tested at 15% strain (a) Schwarz Primitive, (b) Neovius, and (c) IWP.	50
Figure 4.14 Deformation frames of Schwarz Primitive, Neovius, and IWP lattice structures 3D printed using pristine PLA at 0%, 5%, and 10% strain.	51

Figure 4.15 Deformation frames of Schwarz Primitive, Neovius, and IWP lattice structures 3D printed using pristine PP at 0%, 5%, and 10% strain.	52
Figure 4.16 Compressive force-displacement curves of (a) PLA Schwarz Primitive, (b) PLA Neovius, (c) PLA IWP; (d) PP Schwarz Primitive, (e) PP Neovius, (f) PLA IWP structures.....	53
Figure 4.17 Compressive force-displacement curves of 5 vol% Fe/PLA TPMS. ...	54
Figure 4.18 Compressive force-displacement curves of 5 vol% Fe/PP TPMS.	54
Figure 4.19 Simulated compressive stress-strain graph of Pristine PP IWP (40% relative density).....	59
Figure 4.20 Simulated compressive stress-strain graph of 5 vol% Fe/PP IWP.	60
Figure 4.21 Total deformations of compression test modeling of IWP specimens made of 5 vol% Fe/PP composite with (a) 30% relative density, (b) 40% relative density, and (c) 50% relative density.	61
Figure 4.22 Equivalent stress distribution of compression test modeling of IWP specimens made of 5 vol% Fe/PP composite with (a) 30% relative density, (b) 40% relative density, and (c) 50% relative density.....	62
Figure 4.23 Experimentally measured and simulated (FEM) compressive stress-strain curves of the IWP lattice structure with 40% density made of pristine PP. .	63
Figure 4.24 Compressive stress-strain curves for comparison of FEM and experimental.....	64

CHAPTER 1

INTRODUCTION

Since the invention of additive manufacturing (AM), also known as three-dimensional printing (3D printing), many methods and printers have been created to produce components layer by layer. Due to decreased material waste and capacity to produce complex geometries without the use of complicated tools, AM technologies have the potential to result in significant cost savings. As a result, they have received considerable attention during the last decades. One of the most frequently used AM processes for producing components from polymer or composite materials is fused filament fabrication (FFF), also known as fused deposition modeling (FDM). The basic material for this technique is a thermoplastic filament that is continuously fabricated. The molten raw material is extruded from the print head and deposited layer by layer on the build platform. Developments in the FFF technique have made it possible to produce parts with complicated geometries and internal morphologies.

The particle reinforcements constitute a low-cost option for further extruded filaments 3D printable via FDM process. The main target in printing particle-reinforced composite filaments in three dimensions are better tensile/storage modulus, improved wear resistance, and improved dielectric permittivity of the final structures. Particles are rather simple to combine with polymers which enable flexible customization of the composite features to suit a wide range of applications based on several variables. The most crucial properties (mechanical and thermal) of the composites for their use in filament production for AM in general and FDM in particular will be discussed in the following chapters, along with how these parameters can affect them.

In recent years, engineering has witnessed a transformative use of lattice structures, revolutionizing the design, analysis, and production of various components. Lattice

structures, characterized by their interconnected beams, offer a blend of lightweight construction, mechanical robustness, and innovative design possibilities. This thesis aims to explore two prominent types of these namely—Lattice Structures and TPMS (Triply Periodic Minimal Surfaces) lattice structures—focusing on their design, finite element method (FEM) analysis, and additive manufacturing production. Fundamental to this exploration is the comprehension of these structures' characteristics, design principles, and their distinct advantages in various engineering applications. The study also delves into the application of Finite Element Method (FEM) in the design and analysis of lattice structures, aiming to assess their mechanical behavior and optimize design parameters. Additionally, the thesis investigates the manufacturing aspects of lattice structures using additive manufacturing techniques, evaluating the feasibility, challenges, and advancements in producing these intricate designs. As the demand for lightweight, robust, and efficiently designed components grows, this thesis seeks to contribute to the understanding and practical implementation of lattice structures, potentially impacting diverse industries.

This thesis is structured into five main chapters, each covering distinct aspects of the study. Chapter 2 is subdivided into three sections, the first discussing the properties and classification of additive manufacturing techniques, while the subsequent sections detail the production of composite filaments and their application in lattice structure fabrication. Chapter 3 outlines the experimental procedures involved in manufacturing composite filaments, their processing using the FFF method, and subsequent mechanical testing, alongside descriptions of the characterization methods employed. In Chapter 4, the focus is on the experimental results, specifically covering the microstructural examination and mechanical behavior analysis of TPMS lattice parts. Finally, Chapter 5 presents the critical conclusions drawn from the entirety of the study, summarizing the significant findings and insights obtained throughout the research.

CHAPTER 2

LITERATURE REVIEW

2.1 Classification of Additive Manufacturing Techniques

A production technique called additive manufacturing creates nearly net-shaped products directly from CAD models. Due to its freedom from complexity, even though it is a very slow production method when compared to other traditional production methods like casting, molding, and extrusion, it is preferred. Metals, polymers, composite materials, and ceramics are just a few of the materials that can be manufactured using additive manufacturing. In general, the feedstock could also be in powder or filament shape. Production costs could go up depending on the raw materials. Metallic materials, for instance, typically cost more to produce than other materials. This has to do with the fact that metallic materials require a lot of energy to process because they are melted, sintered, or sprayed on the substrate or layers. As shown in Figure 2.1, AM can be split into a number of different technologies, including binder jetting, stereolithography, electron beam melting, selective laser sintering, and fused deposition modeling (FDM). Plastics, metals, ceramics, and composites are materials that can be used in additive manufacturing, depending on the technology. However, the supply of materials that are appropriate for use in additive manufacturing is still quite limited. In order to fill this gap, researchers are attempting to introduce novel materials and materials prepared/processed to achieve the aforementioned characteristics. As in many situations, certain special characteristics are required, such as mechanical strength, electrical conductivity, thermal endurance, durability, and multi-functionality [1].

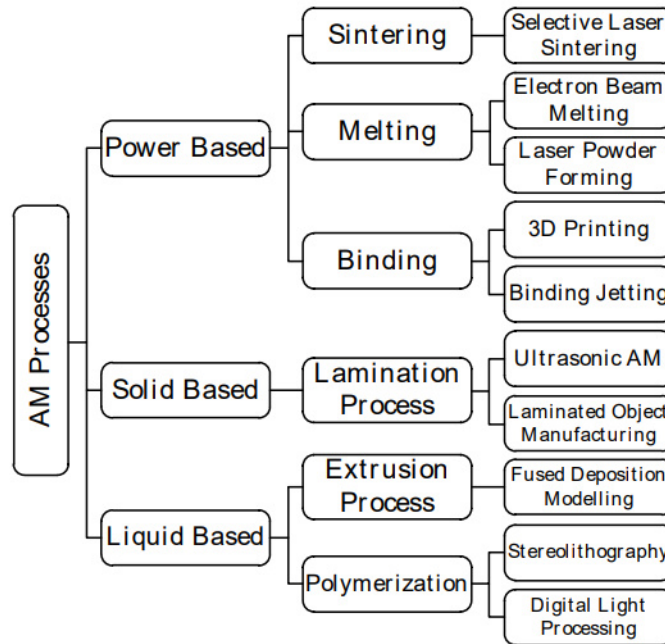


Figure 2.1 Classification of Additive Manufacturing Processes [1].

2.1.1 Powder-Based Additive Manufacturing Techniques

A sort of 3D printing technology called powder-based additive manufacturing uses successive layers of powdered material to fuse or bond together to form three-dimensional objects. Selective laser sintering, selective laser melting, selective electron melting, and binder jetting are the four primary methods of powder-based additive production. A laser is used in the additive manufacturing process known as selective laser sintering (SLS) to selectively fuse or sinter subsequent layers of powdered material, usually made of plastic, metal, or ceramic. The powdered substance is heated by the laser to a temperature just below its melting point, fusing it together and causing it to solidify into an object layer by layer. Functional prototypes, low-volume production components, and intricate geometries are frequently produced using SLS [2].

Similar to selective laser sintering (SLS), selective laser melting (SLM) fully melts the powdered material as opposed to merely sintering it. SLM is ideally suited for

the production of high-performance components in aerospace, automotive, and medical applications because this yields a completely dense and homogenous part (Figure 2.2) [3].

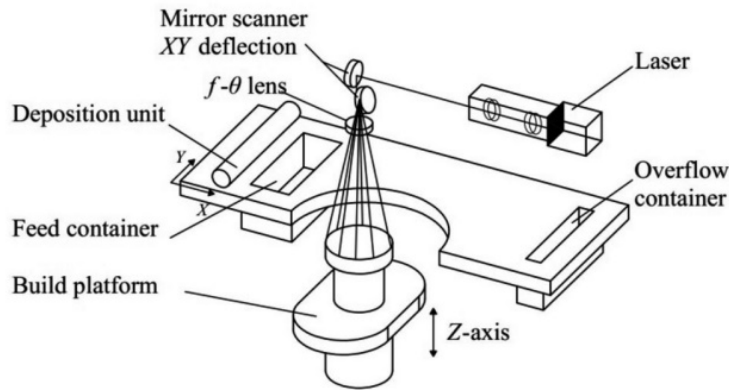


Figure 2.2 Typical SLM configuration schematic [4].

The powdered material, which is usually a metal alloy, is melted using a technique called selective electron melting (SEM), also referred to as electron beam melting (EBM). Layer by layer, the powder is melted as the beam is directed onto the powder bed. To avoid material contamination, the procedure is carried out in a vacuum. SEM is frequently used in aerospace and medical uses because of its propensity for creating high-strength, high-performance parts with intricate geometries [4].

A liquid binding agent is used in the powder-based additive manufacturing method known as "binder jetting" to specifically bond subsequent layers of powdered material, usually metal or ceramic. Layer by layer, the binder is jetted onto the powder bed, joining the individual particles to form a solid structure. The procedure is suitable for producing large, complicated parts because it is reasonably quick and affordable. However, compared to parts created by other powder-based additive manufacturing processes, the end products are usually less dense and stronger [5].

Overall, additive manufacturing techniques based on powder are flexible, enabling the creation of parts with intricate geometries and a variety of materials, such as

metals, plastics, and ceramics. Depending on the desired properties of the finished product, each of the four primary kinds of powder-based additive manufacturing is appropriate for a different application due to its own strengths and weaknesses.

2.2 Solid Based Additive Manufacturing Techniques

Based on sheet lamination, several additional methods have been created that use different construction materials and cutting techniques. The sheets can either be cut and then stacked or stacked and then cut due to the building principle, which only requires the outer contours of the parts to be cut. These procedures can be further divided into the following categories: gluing or sticky bonding, thermal bonding, clamping, and ultrasonic welding. An extensive discussion of this bonding method is included at the end of this chapter because using ultrasonic welding includes distinctive solid-state bonding characteristics and can facilitate various applications [6].

2.2.1 Liquid-Based Additive Manufacturing Techniques

2.2.1.1 Lithography-based 3D print using photopolymer

Liquid photopolymer resin is precisely controlled to solidify in lithography-based 3D printing technology. The designed 3D object is produced by separating the solidified component from the uncured liquid resin. SLA, Digital Light Processing (DLP), and Two-Photon Polymerization (2PP) are categorized as the most popular techniques based on the various light sources used to cure liquid material. The first 3D printing technique, SLA, solidifies liquid resin using a narrowly focused laser.

Computer software is used to draw the designed outline before the first layer of the print is solidified on a movable platform. The platform will then descend into the resin tank for a distance equivalent to one layer's thickness, typically between 10 and 200 micrometers. The resin surface will then be recoated with a thin liquid resin coating

using a coater. Until the entire designed 3D object is printed, successive layers will be drawn on top of the previous layers using the same solidification-descending-recoating method. The platform will be elevated after printing [7].

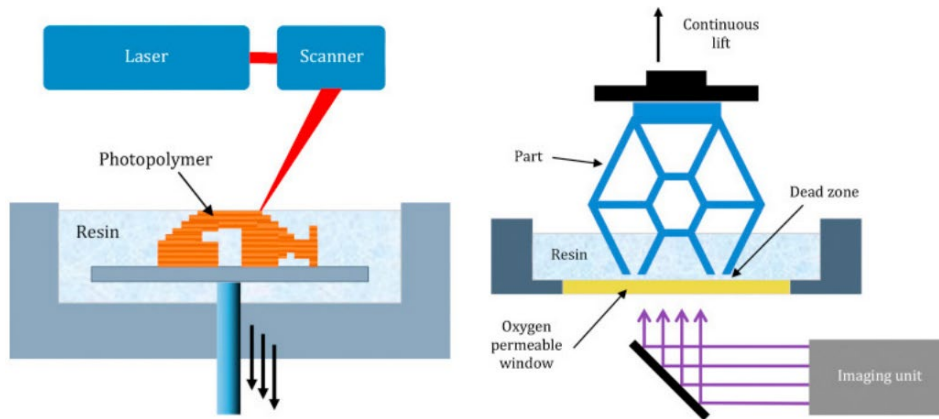


Figure 2.3 Lithography-based 3D print technologies: (left) SLA, (right) DLP [8].

The platform will raise to a single-layer height after printing the first layer. The succeeding liquid resin layer is between the first layer and the floor of the resin vat.

The image projection and platform-raising procedure will be repeated until the 3D object is printed. Compared to the traditional top-up SLA strategy, the above-mentioned bottom-up approach can significantly reduce the volume of resin needed for SLA technology [8].

2.2.1.2 Fused Deposition Modelling (FDM)

The fused deposition modeling (FDM) or fused filament fabrication (FFF) method is an additive manufacturing method that produces nearly net shapes directly from the CAD model. Additive manufacturing (AM) via extrusion of metallic powder contained in a polymeric matrix can provide the way complex metallic models are fabricated. Fused filament fabrication of metals saves material and reduces cost [9].

Selective Laser Sintering (SLS) is an alternative additive manufacturing method for FDM. However, a high-energy laser is used as a heat source in the SLS method. So, the processes cost more than FDM [10]. One of the most common AM techniques is FFF.

Thermoplastics and their composites are typically used as filament materials for part manufacturing. Researchers are still developing new filament materials in an effort to enhance component characteristics. FFF build parts are still used in various applications despite numerous chances to improve their characteristics (Figure 2.4). Nowadays, additive manufacturing techniques are inevitable in various industries such as aerospace, automobile, and biomechanical engineering. There have been numerous chances in recent years to use AM techniques in the medical industry. As each patient needs specific implants, tools (such as drilling guides), supportive guides, and prostheses, there is a high demand for the development of customized products in the medical industry. The AM processes effectively create customized goods with high precision and accuracy at a reasonable price. The applications of additive manufacturing (AM) in the medical sector include tissue engineering, prosthetics, splints, implants, tools and instruments for medical devices, medical aids, and medical models. Typically, patient anatomy is captured for scaffolds and implants using computed tomography (CT) or other 3D image scanning methods. CT datasets may be utilized to create a 3D model for AM methods to use in printing [11].

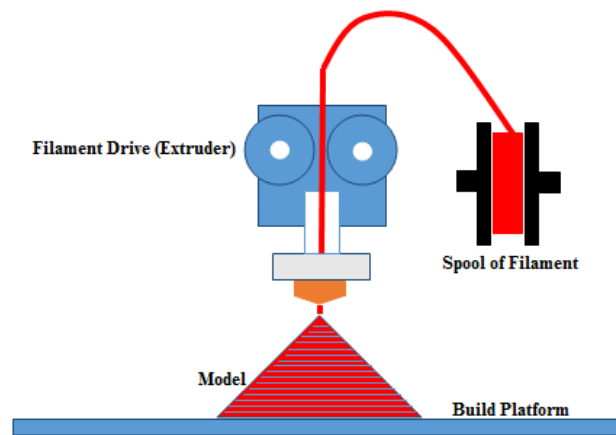


Figure 2.4 Schematic representation of Fused Filament Fabrication methods [11].

The extruder typically travels in a horizontal plane while printing in most FFF machines or printers by the pre-generated tool path for depositing a layer. The build platform shifts in the lower z-direction after a layer is deposited. It continues until the component is finished being constructed, with the following layer being deposited over the preceding layers. Bonding between two successive layers is what gives a built-in component its power. For the surface of the previously deposited layer to become activated and for the freshly deposited layer and the activated surface to become adherent, sufficient heat energy is needed.

The extruder typically travels in a horizontal plane while printing in most FFF machines or printers by the pre-generated tool path for depositing a layer. The build platform shifts in the lower z-direction after a layer is deposited. It continues until the component is finished being constructed, with the following layer deposited over the preceding layers. Bonding between two successive layers is what gives a built-in component its power. For the surface of the previously deposited layer to become activated and for the freshly deposited layer and the activated surface to become adherent, sufficient heat energy is needed [11].

(i) Pure Thermoplastic Filaments

For the FDM process, there are numerous thermoplastic materials available as filaments. Filament extruders, such as Filabot extruders, accomplish the fabrication

of filaments from thermoplastics and composites. Figure 2.5 displays a typical filament extruder.

The raw materials (thermoplastics and composites) are fed into the barrel for the filament-creation process through a hopper in the form of granulates or pellets. The barrel serves as a casing for the rotating screw(s). In the barrel, the raw materials are also heated. Feed, transition, and metering zones comprise the barrel's three zones [12]. The raw materials become plasticized in the transition zone, soften in the feed zone, and melt entirely in the metering zone. The input materials are used to determine the temperatures at various zones. The input materials move through the revolving screw's surface from the feed zone to the transition zone, then to the metering zone. There may be one or two screws inside the barrel. The twin-screw extruder is known as a single-screw extruder, but the former has just one screw. From the metering zone, the raw materials that have melted are extruded through a die. The die's diameter is chosen based on the necessary filament diameters; for 1.75 mm filaments, a brass die with a diameter of 2.5 to 3.5 mm is typically used [9].

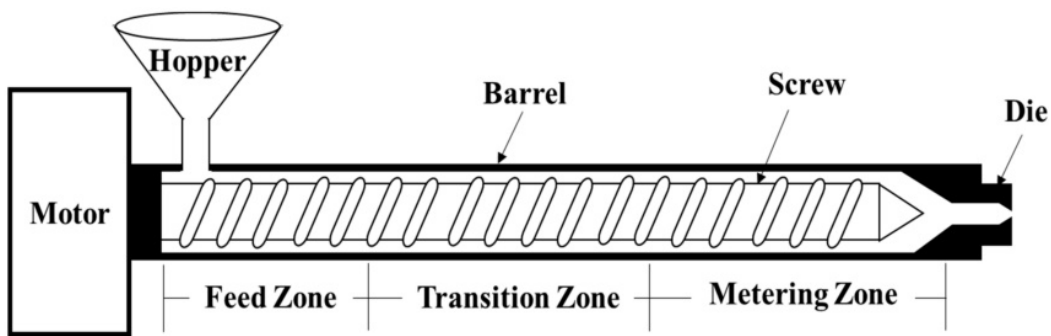


Figure 2.5 Schematic representation of Fused Filament Fabrication Extruder [12].

The choice of filament material for the FFF method is typically determined by the application or other built-part requirements because different thermoplastics have varied qualities.

Acrylonitrile butadiene styrene (ABS) and polylactic acid (PLA) are the most popular and often used filament materials for the FFF method [13]. Both materials have strengths and weaknesses. As ABS melts at high temperatures, it is known to release toxic fumes, shrink significantly as it cools, and is not environmentally friendly. However, PLA is regarded as biodegradable and has high brittleness, low mechanical characteristics, and low heat resistance. To create useful 3D-printed parts, many thermoplastic filaments are used. Accordingly, depending on the application of interest, these thermoplastic filaments must achieve various qualities, including chemical resistance, biocompatibility, heat resistance, flexibility, and strength. Before using them in a particular FFF process, it may be worthwhile to be aware of a particular property that some pure thermoplastic filaments have. Majority of the pure thermoplastics used as FFF filaments are readily available commercially, and their succinct descriptions are included below:

One of the most widely utilized filament materials is Acrylonitrile Butadiene Styrene (ABS) [14]. Even though ABS, an amorphous polymer, is not thought to degrade naturally, it is valued for its beneficial qualities, such as strong impact resistance, abrasion resistance, and chemical resistance. The hardness of ABS is another benefit. ABS also has significant drawbacks, namely warping and shrinkage during and after part creation [14, 15]. ABS typically has a melting point between 200–250 °C. Those with chemical sensitivity or breathing issues may be harmed by the toxic vapors produced by ABS [16]. A few valuable components were created using ABS in the automotive, medical, and aerospace industries [17].

Polylactic acid (PLA): PLA is another common thermoplastic known for its biodegradability but also known for its sensitivity to humidity over 60 °C. PLA build parts are often reported to experience lower distortions during printing than ABS, but they have low thermal conductivity and toughness [17]. PLA build parts are typically used for practical applications that require a certain degree of aesthetic characteristics [18].

Polycarbonate (PC): This transparent material is renowned for its high glass transition temperature, robust mechanical characteristics, and transparency. Moreover, like ABS, they are amorphous. While polycarbonates have high print temperatures and are susceptible to damp, they are not as durable. The automobile and aerospace industries have used PCs because they can print working prototypes [19].

Polyether ether ketone (PEEK) has a glass transition temperature of about 143 °C. It has a reputation for being biodegradable, lightweight, chemical and heat resistant, and having great mechanical strength. PEEK may be printed at a relatively high temperature of about 340 °C [20].

Polyetherimide (PEI) is a lightweight thermoplastic with excellent mechanical characteristics and resistance to heat and smoke. It has a high glass transition temperature and is a biocompatible polymer. Poor surface polish and dimensional precision characterize FDM items made from PEI. Rapid prototyping applications in various industries, including aerospace and automotive, would be an excellent fit when considering the weight-to-strength ratio [21].

Nylon: Nylon is a flexible, heat- and impact-resistant material. It is resilient and also has strong toughness ratings. As a hygroscopic material, it absorbs much moisture, which lowers the quality overall. Like ABS, nylon is susceptible to warping. The warping impact can be minimized by maintaining the bed temperature at roughly 75 °C [22].

High-impact polystyrene (HIPS) is a biodegradable thermoplastic material with low strength and favorable machining properties. This FDM filament has high flow properties, is impact-resistant, and is inexpensive. However, it is prone to wear and needs a hot build platform and high printing temperature. HIPS is lighter than ABS but has qualities that are similar to ABS. HIPS dissolves with compounds like limonene, making it a better choice for support structures [23].

Due to financial constraints, pricing is a crucial consideration when choosing filament materials together with the qualities of those materials. The process used to prepare the filament, the location of the manufacturing facilities, the cost of labor, the quality of the materials, and other costs associated with raw materials, production, and logistics all affect the price of the filament. The best filament for a given application should be chosen based on the material's characteristics while keeping in mind the use or functioning of the printed pieces. Medical implants and food packaging can both be made with PLA-based filaments. On the other hand, ABS and HIPS are advantageous for applications requiring strong impact resistance. Nylon is a ductile, strong, and wear-resistant filament material. Low-quality filaments typically are not a problem for aesthetic reasons. To choose a material for a functional part, it is essential to analyze the filament materials' properties.

Additionally, it should be noted that filament mechanical and thermal characterizations, electrical resistance, and fatigue behaviors can differ between producers and users. The quality of the raw materials, the fabrication steps, the pre- and post-treatments of the materials, or the testing circumstances are only a few examples from the filament producers' point of view of external elements contributing to this difference. The condition of the FFF equipment, the settings for the process parameters, the management of the materials before and after printing, and the circumstances surrounding filament storage are a few examples from the viewpoint of the filament users.

(ii) Composite Filaments

Pure thermoplastic filaments now in use have drawbacks such as low strength and stiffness when fulfilling the enhanced performance of FFF construct parts. High temperatures cause thermoplastics to soften and lose their ability to take on their original shape. Often, a product made from thermoplastic filaments cannot satisfy a particular set of functional specifications. Compared to injection molded components' characteristics, the properties of FFF-built parts are frequently insufficient [24]. FFF filament materials that are compact, strong, and have excellent

surface quality are constantly being sought after based on application fields. Composite materials are considered an excellent solution to fulfill these requirements. Several reinforcements can be applied to pure thermoplastics to achieve the desired characteristics of an FFF construction part.

Additionally, adopting composite materials is motivated by the need for novel and environmentally friendly materials. Compared to pure polymers, composite materials have reportedly been shown to have better characteristics. The filaments needed for the FFF machine must have particular form, ductility, and other qualities. Material selection for FFF composite filament is difficult since nozzle clogging and filament breakage are possible during the FFF method's part manufacturing [25]. Additionally, composite materials are difficult to recycle after their useful lives due to their heterogeneous composition. When choosing reinforcement and matrix composition for composite filaments, environmental consequences such as carbon footprints and others should be considered. The carbon footprint of bio-based and biodegradable reinforcements and matrices is typically reduced near the end of their life cycle. As seen in Figure 2.6, several kinds and shapes of reinforcing materials are employed as filaments for composites. Based on the forms of reinforcement, the composite materials for FFF filaments are segmented in this area.

The adverse effects of producing polymer matrix composite filament for 3D printing on the filament's quality and mechanical properties can include:

1. **Poor Printability:** Adding fillers and reinforcements to the polymer matrix can result in poor printability due to clogging or nozzle blockage during the 3D printing process.
2. **Reduced Strength:** Incorporating fillers and reinforcements can also reduce the printed object's strength and stiffness due to weak bonding between the polymer matrix and the fillers.

3. **Reduced Flexibility:** Adding fillers and reinforcements can reduce the flexibility of the printed object, making it more brittle and prone to cracking or breaking under stress.

4. **Poor Surface Finish:** The presence of fillers and reinforcements can also result in a rough surface finish on the printed object, which may require additional post-processing steps to achieve the desired smoothness.

5. **Inconsistent Properties:** The properties of polymer matrix composite filament can be highly dependent on the manufacturing process, resulting in inconsistent properties between different batches of filament. This can lead to variations in the final printed object's quality and mechanical properties.

These adverse effects can impact the overall quality and mechanical properties of the 3D-printed object, making it less suitable for specific applications or requiring additional processing steps to achieve the desired properties.

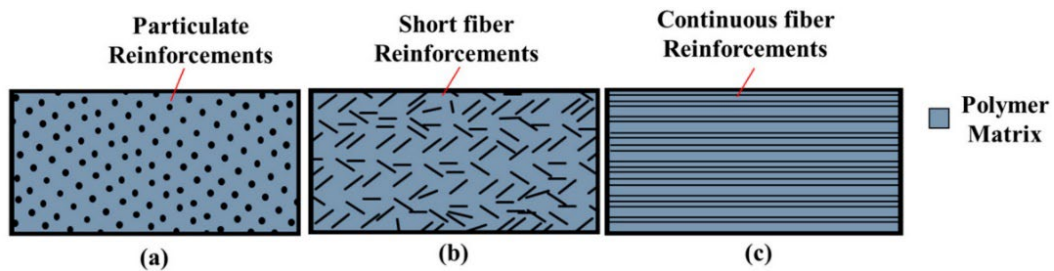


Figure 2.6 Different reinforcement materials are utilized in composite filaments: (a) Particulate reinforcement, (b) short fiber reinforcement, and (c) continuous fiber reinforcement composites [12].

(iii) Particulate Composite Filaments

The reinforcement materials are combined with a polymer matrix and then extruded into FDM filaments to create particulate composite filaments (Figure 2.6 a). The size, shape, orientation, volume percentage, and interfaces between the particles and the polymer matrix all affect the properties of particulate composites. Due to the brittleness of the filaments and the large particle size, the FDM process frequently encounters two typical technical issues: filament breakage and nozzle clogging.

When creating or making use of particle composite filaments, various technological issues must be taken into account. The effects of particle size, volume percentage of particles, and process factors on part qualities can be significant in addition to the technical concerns. A composite material's selection depends on its manufacturing potential and component qualities. The ability of the composite filaments to be incorporated into conventional FDM machines without further hardware and software modification is necessary to guarantee the widespread use of particle composite filaments in the FFF process [26].

(iv) Short Fiber Composite Filaments

The matrix is combined with short fibers before creating the short-fiber composite filaments. Short fiber composites have their fibers evenly distributed across a matrix, as seen in Figure 2.6 b. Utilizing a single screw or double screw extruder, the mixed material (such as pellets) is used to create a filament. An experimental examination shows composite built parts have significantly higher tensile modulus, stiffness, Poisson ratio, and shear modulus. The tensile strength and shear strength, however, did not alter significantly. It shows that there was insufficient adhesion between PLA and carbon fibers and stress sustained by the matrix material when the load was applied. The mechanical characteristics of composite build FFF pieces are also thought to be significantly influenced by the build orientation and fiber length. Kamaal et al. studied the mechanical characteristics of PLA-CF composites and demonstrated that layer thickness and infill density significantly influence building orientation and process parameters [27].

(v) Continuous Fiber Composite Filaments

Figure 2.6 shows how the fiber alignment typically appears in continuous fiber composites. Reinforcements and polymer matrix are mixed during the manufacturing of filaments for particle and short fiber composites. Additionally, the filaments are made from the mixture using various tools, including a single screw extruder in the FDM method. However, the FDM technique uses two distinct spools to deposit the matrix polymer and fibers for continuous fiber composite filaments.

Continuous carbon fibers' effects on the tensile strength and flexural strength of FFF-built PLA pieces were examined by Li et al. According to experimental study, the tensile strength and flexural strength of composite build parts are 185% and 11% higher, respectively, than those of pure PLA build parts. Because there is insufficient adhesion between PLA and carbon fibers, it may be said that the flexural strength has not changed significantly. In order to increase the adhesion between PLA and carbon fibers, which in turn increased flexural strength, the surface of the carbon fibers was changed using methylene dichloride solution, PLA particles, and deionized water [28].

2.3 Lattice Structures

An array of face-and-edged spatial periodic unit cells forms a lattice structure, an architectural design. There are cellular solids, two- and three-dimensional lattice formations, and more. Because the microarchitecture makes it possible to think of it as a monolithic material with its own unique set of valuable qualities, it is also known as a lattice material. Lattice structures have many superior qualities that make them a promising option for a variety of applications, such as a lightweight structure due to its high specific stiffness and strength, a heat exchanger due to its large surface area, an energy absorber due to its ability to undergo great deformation at a relatively low-stress level, and an acoustic insulator due to its numerous internal pores. Lattice structures have been created using various standard manufacturing techniques, such as investment casting, deformation forming, and metal wire procedures. However, these procedures rely on complex machinery with exact process control and additional assembly or bonding phases to produce the desired structures. Additionally, using these processes severely restricts the types of designs that can be used. Because of its distinctive characteristics, additive manufacturing (AM) is a good choice for producing items with lattice structures. As shown in Figure 2.7

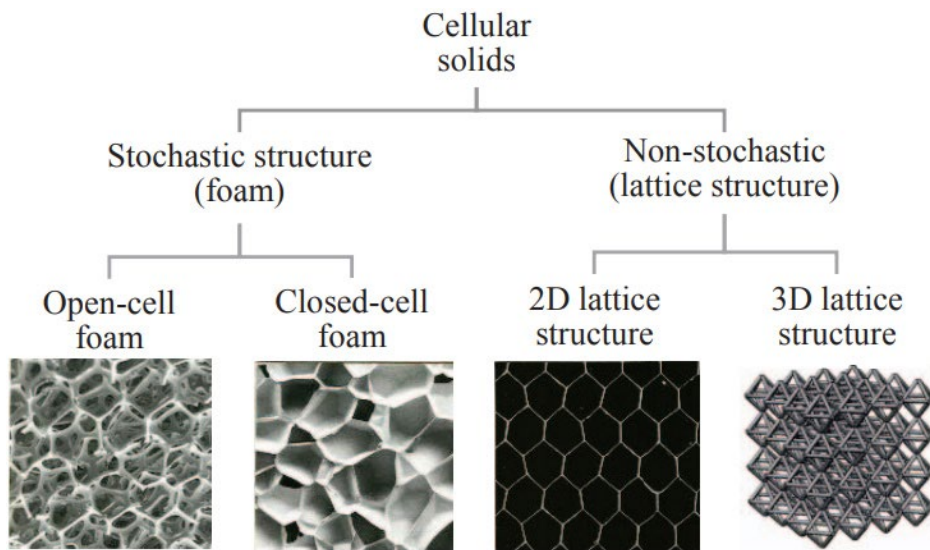


Figure 2.7 Classification of Cellular Solids [29].

Lattice structures have been created using various AM techniques, and their manufacturability has been examined. To make the theoretical technology applicable in the industrial setting, some design approaches for lattice structures have been put forth, and several specialized software tools have been created. The choice of material, architecture, and porosity must be considered the mechanical behavior of lattice structures. AM lattice structures are particularly appealing to various applications due to their functional flexibility, which reduces the amount of material used in the production process, shortens the time required to make an object, uses less energy in the production process, and increases the strength of the produced thing while reducing its weight [29]. Lattice structures fill a void in the advanced material industry. They not only meet the demands of reducing weight, energy, and time but also enable the utilization of additional incredibly advantageous side effects.

Some of these are energy absorption, vibrational and acoustic dampening, high strength-to-weight ratios, and thermal management skills. Lattice structures are well known for their capacity to absorb energy. Hollow trusses are another method for utilizing the energy-absorption property of lattice structures. Because they have a higher second moment of inertia than solid trusses, hollow trusses are employed in constructing lattice structures and have been shown to have a higher load-carrying

capability in a specimen. In addition, lattice constructions are well known for maintaining relatively high levels of strength yet being lighter than an equivalent solid object. Lattice structures' relative strength can be raised in several different ways that have been found to work. These processes include producing materials with dimensions that are only a few microns wide, resulting in greater strength than a pure solid material.

2.3.1 Triply Periodic Minimum Surface (TPMS) Lattice

Recent years have seen a substantial increase in study interest in triply periodic minimum surface (TPMS) structures because of their exceptional mechanical qualities. A group of surfaces known as TPMS have zero-mean curvature at all points on the surface and a large surface area. The surface is divided into two endless, non-intersecting, interlaced domains while retaining open cavities. This kind of surface can be periodically replicated in three perpendicular directions. The distinct geometry of surface-based lattices (TPMS) reduces stress concentration compared to truss-based lattices, resulting in a smoother crush behavior when subjected to compressive loads. For instance, Khaderi et al. [30] found that the Gyroid-lattice's elastic and plastic properties suffer a severe knock-down due to flaws in the structure. The TPMS-CMs are devoid of joints and struts. The TPMS-CMs' connectedness and continuity enable a smoother transfer of loads (see Figure 2.8) [31], which improves the TPMS-CMs' integrity compared to truss/strut-based CMs with joints.

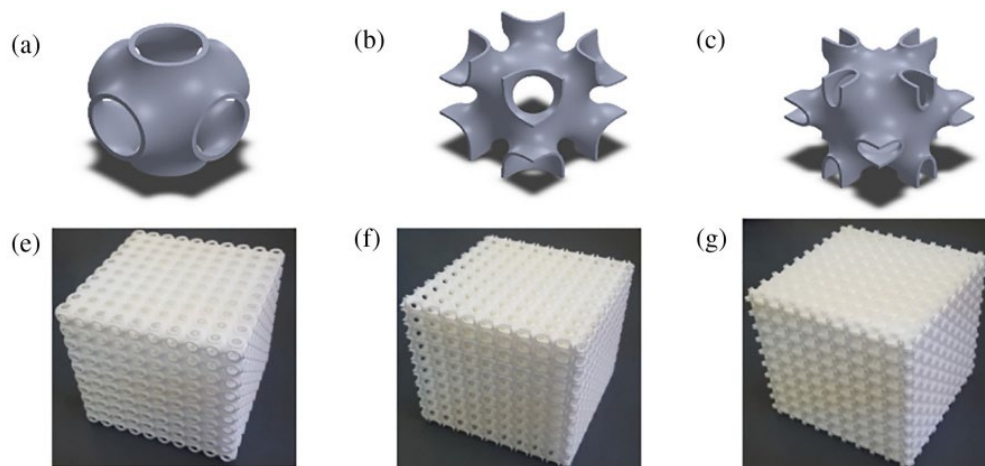


Figure 2.8 TPMS-CMs with a 10% relative density, as shown in CAD drawings: (a) Primitive-CM, (b) IWP-CM, and (c) Neovius-CM, respectively. 3D-printed samples of the relative densities for (e) Primitive-CM (23.5%), (f) IWP-CM (25.6%), and (g) Neovius-CM (23.7%) [31].

The traditional techniques for preparing materials for cellular structures include wire mesh preparation, template replication, space holders, and gas injection. However, these methods are limited to the fabrication of stochastic foams with considerably low uniformity or simple 3D wire mesh with high cost. The limitations mentioned above can be addressed by applying additive manufacturing (AM) technologies for fabricating cellular materials with designed complex structures. The development of additive manufacturing (AM) technologies, particularly laser beam powder bed fusion (LB-PBF), in which an energy source selectively melts the metallic powder, has made it possible to fabricate such complicated structures. In addition to LB-PBF, the FDM method could be an alternative to fabricating polymeric and polymer matrix composite TPMS [32-33].

CHAPTER 3

EXPERIMENTAL WORK

Experimental works conducted in this study mainly consist of three steps. The first step is preparing pristine and composite fully dense cubic test specimens and their mechanical testing. Flowchart related with fully dense specimen preparation is shown in Figure 3.1. In the second step, Triply Periodic Minimal Surface (TPMS) specimens were produced by Fused Filament Fabrication (FFF), and the mechanical properties of the specimens were determined. Flowchart related with the preparation of the TPMS specimens is shown in Figure 3.2. Finally, modeling of compression tests of TPMS structures has been conducted via FEM. Flowchart related with modelling of TPMS specimens is shown in Figure 3.3. In Table 3.1 materials used in the production of TPMS specimens and the experimental matrix of the current study is provided.

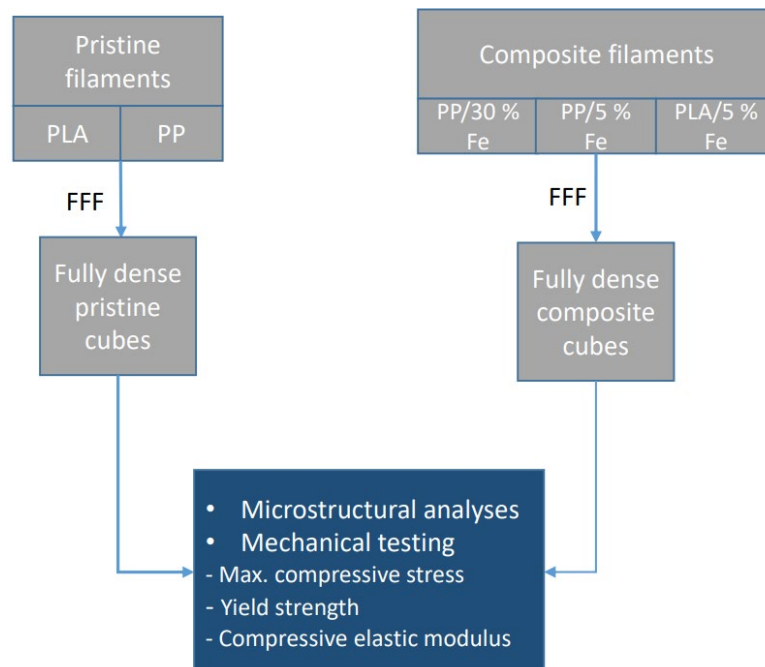


Figure 3.1 Fully dense cubic specimen preparation steps.

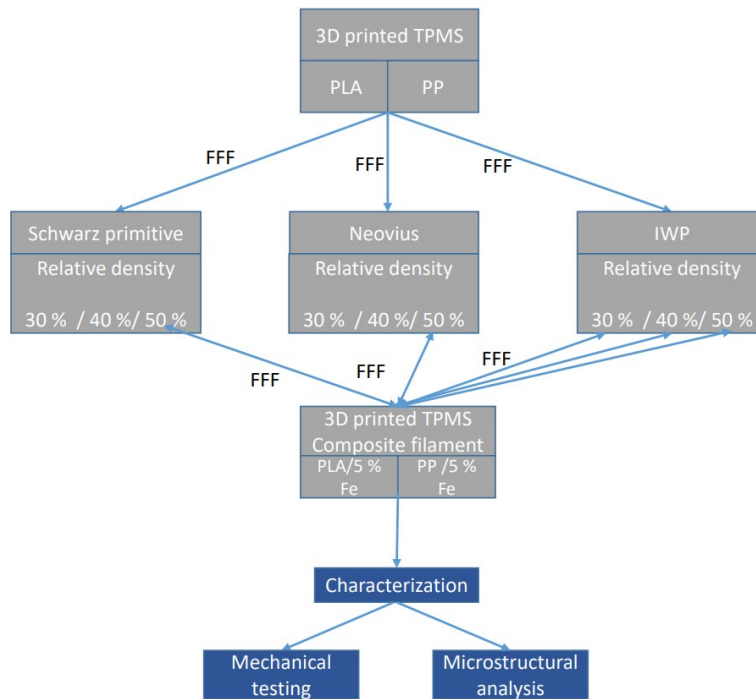


Figure 3.2 TPMS specimen preparation steps.

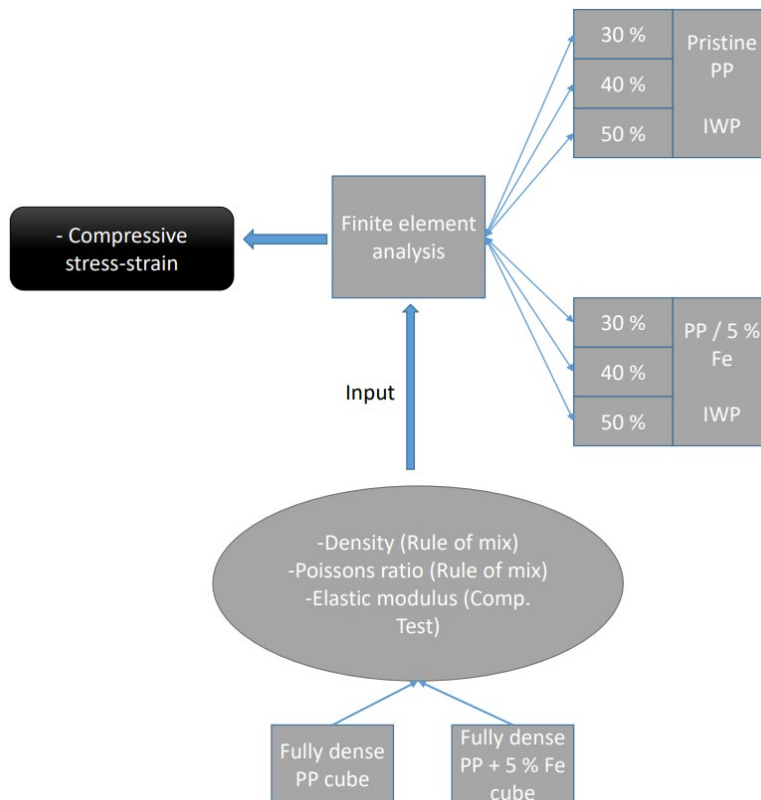





Figure 3.3 Modelling of TPMS specimens with Finite Element Analysis.

Table 3.1 Materials used for the production of TPMS.

	TPMS	Schwarz Primitive	Neovius	IWP
Rel. dens.				
30%		- Pristine PLA - Pristine PP	- Pristine PLA - Pristine PP	- Pristine PLA - Pristine PP - 5 vol% Fe/PLA - 5 vol% Fe/PP
40%		- Pristine PLA - Pristine PP	- Pristine PLA - Pristine PP	- Pristine PLA - Pristine PP - 5 vol% Fe/PLA - 5 vol% Fe/PP
50%		- Pristine PLA - Pristine PP - 5 vol% Fe/PLA - 5 vol% Fe/PP	- Pristine PLA - Pristine PP - 5 vol% Fe/PLA - 5 vol% Fe/PP	- Pristine PLA - Pristine PP - 5 vol% Fe/PLA - 5 vol% Fe/PP

3.1 Starting Materials

Two primary polymeric materials were used in this study as a filament. The first one is Polylactic acid (PLA), and the second one is Polypropylene (PP). 1.75 mm diameter filaments (PP/PLA, Filameon, Kayseri, Turkey) were utilized.

Reinforcement materials used for polymer matrix, particulate composite filaments, were gas-atomized Fe powders. The particle size distribution of the powders measured using the Malvern Mastersizer 2000 module is shown in Figure 3.4. The particle size range of the metallic powder was determined to vary between 0.02 and 2000 μm , with volume-weighted mean particle size of roughly 93.22 μm .

In order to obtain refined powder size, sieve analyses were also done using a 270 mesh / 53 μm size sieve.

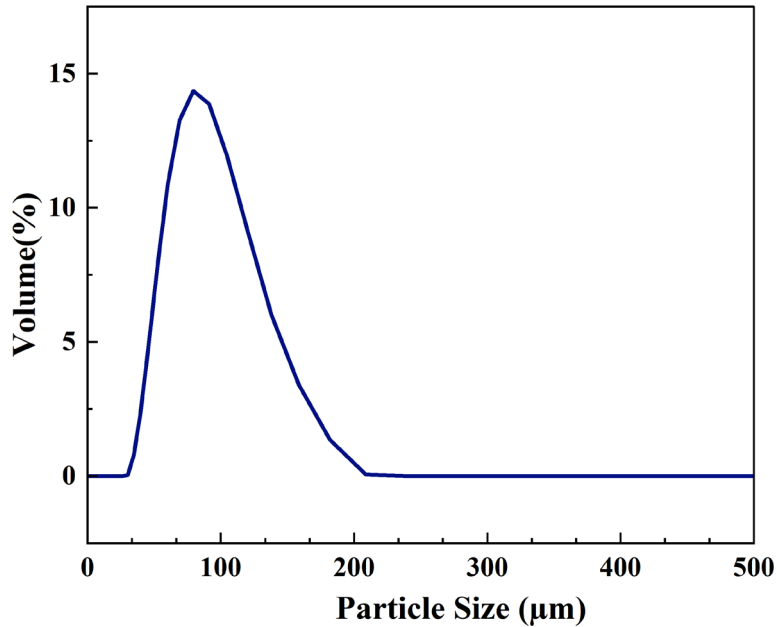


Figure 3.4 Particle size distribution of the Fe powders used in this study.

3.1.1 Composite Filament Production

Composite filament production for Fused Filament Fabrication (FFF) method has two steps. The first step is producing composite pellets with sieved metallic powder and polymeric matrix. The second step is producing composite filaments by extrusion with a specific diameter. In this study Fe particles have been incorporated in two different polymers to obtain two different metal/polymer composite filaments. One of the composite filaments was PLA based, and the other was PP based. Thermoplastic polyurethane (TPU) was used as a plasticizer to develop plastic behavior and printability of the composite filaments because adding reinforcement material deteriorates filaments' mechanical properties and printability. Plasticizers can increase the flexibility of composite filaments making them more suitable for applications which require a certain degree of flexibility or bendability. Plasticizers

can also improve the printability of composite filaments by reducing the risk of clogging or nozzle blockage during the 3D printing process.

Furthermore, another critical problem with composite filament production is the degradation of the mechanical properties, especially the strength, of the final 3D-printed parts. Incorporating fillers and reinforcements may reduce the strength and stiffness of the printed object due to weak bonding between the polymer matrix and the fillers. Surfactants can improve the bonding between the polymer matrix and the fillers in composite filaments by reducing the interfacial tension between two materials enhancing their compatibility and promoting bonding. In this study, stearic acid has been used as the surfactant for promoting surface compatibility and bonding between the metallic particles and polymer matrices of the composite filaments.

In order to create composite blends, twin screw extruders shown in Figure 3.5 (a) were used. The first screw is used to obtain composite granules. The hot blend was obtained at nearly 190 °C with 7 cycle/min feeding period and 7 cycle/min screw turning period. Water was used to cool down the composite blends to room temperature. After cooling down to room temperature, composite blends with granule form have been obtained (Figure 3.5 (b) (c)). The second screw is used to mix composite granules and additional polymers. After mixing and melting of the compound in the extruder, filament winding operation is done (Figure 3.5 (d) (e)).

PP based composite blends with two different metallic particle contents have been used to produce two different composite filaments. The first filament contained nearly 30.80 vol% metallic powder, and the second filament had nearly 5 vol% metallic powder. The composition and density of the composite filaments produced by extrusion with the first two batches are given in Table 3.2 and Table 3.3 in terms of weight and volume percentage.

Table 3.2 Composition and density of the filament produced by the first batch.

Property	Fe	PP	TPU	Stearic Acid
Mass (g)	228	52.0	10.0	1.00
Volume (cm³)	29.0	55.3	8.50	1.10
Density (g/cm³)	7.86	0.94	1.18	0.94
wt%	78.4	17.8	3.44	0.35
vol%	30.8	58.8	9.05	1.17

Table 3.3 Composition and density of the filament produced by the second batch.

Property	Fe	PP	TPU	Stearic Acid
Mass (g)	998.22	2183.93	144.00	9.30
Volume (cm³)	127.00	2323.33	80.00	9.90
Density (g/cm³)	7.86	0.94	1.18	0.94
wt%	29.92	65.47	4.31	0.27
vol%	5.00	91.74	3.14	0.34

In the third batch, PLA was used instead of PP as the polymer matrix of the composite filament (Figure 3.5). TPU was used to increase the plasticity, formability, and printability of the final filament, and stearic acid was used as a surfactant for metallic powder (Table 3.4).

Table 3.4 Composition and density of the filament produced by the third batch.

	Fe	PLA	TPU	Stearic Acid
Mass (g)	998.2	2904.1	144.0	9.30
Volume (cm³)	127.0	2323.3	80.00	9.90
Density (g/cm³)	7.86	1.25	1.18	0.94
wt%	24.61	71.60	3.55	0.23
vol%	5.00	91.74	3.14	0.34

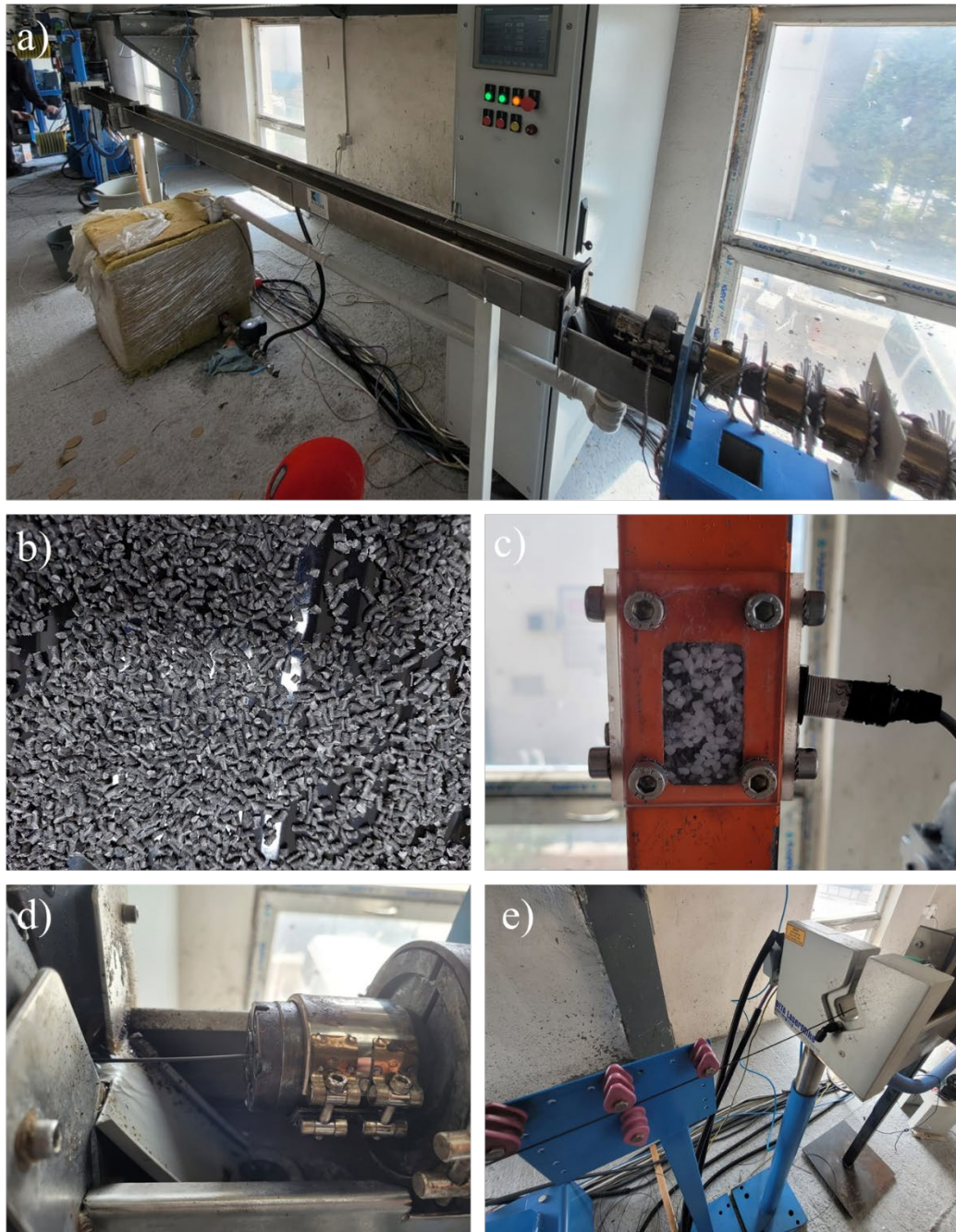


Figure 3.5 Composite filament production set-up; (a) twin screw extruder setup, (b) composite granules, (c) charging granules to extruder, (d) and (e) filament winding.

3.1.2 Production of the Cubic Specimens

Unlike TPMS lattice structures, fully dense cubic specimens have been produced with $10 \times 10 \times 10$ mm sizes for material testing. Cubic structures were produced using FFF with pristine polymer filaments (PLA and PP) and with 3 different metal/polymer composite filaments (30.80 vol% metal/PP, 5.00 vol% metal/PP, 5.00 vol% metal/PLA).

3.1.3 Mechanical Characterization of Cubic Specimens by Compression Test

Static uniaxial compression loading tests were conducted on fully dense cubic specimens, comprised of either pristine polymer or composite filaments. The experiments were performed utilizing an Instron 5582 universal testing device equipped with a 50 kN load cell. In the tests, the load was applied parallel to the building direction.

3.1.4 Producing of the TPMS Lattice Structures with FFF

Each TPMS model is designed according to a mathematical equation. In this study, ANSYS software was used to generate TPMS geometries. This software contains algorithms that allow the formation of various lattice structures. 3 different designs (Schwarz Primitive, IWP, and Neovius) were completed by applying the below equations and setting the variable t as 0. According to Zheng et al. [35], the mechanical performance of the TPMS lattice structures is optimal when $t=0$.

$$\text{Schwarz Primitive} : \cos x + \cos z + \cos y = t \quad (\text{Eqn. 3.1})$$

$$\begin{aligned} \text{IWP} : \cos x \cdot \cos y + \cos y \cdot \cos z + \cos z \cdot \cos x - \cos x \cdot \cos y \cdot \cos z \\ = t \end{aligned} \quad (\text{Eqn. 3.2})$$

$$Neovius : 3(\cos x + \cos y + \cos z) + 4\cos x \cdot \cos y \cdot \cos z = t \quad (Eqn. 3.3)$$

The sizes of the internal cavities in the lattice structures have been changed to obtain varying relative densities. Consequently, lattice structures with 3 different relative densities (30%, 40%, and 50%) having external dimensions of $40 \times 40 \times 40$ mm and $20 \times 20 \times 20$ mm were designed (Figure 3.6).

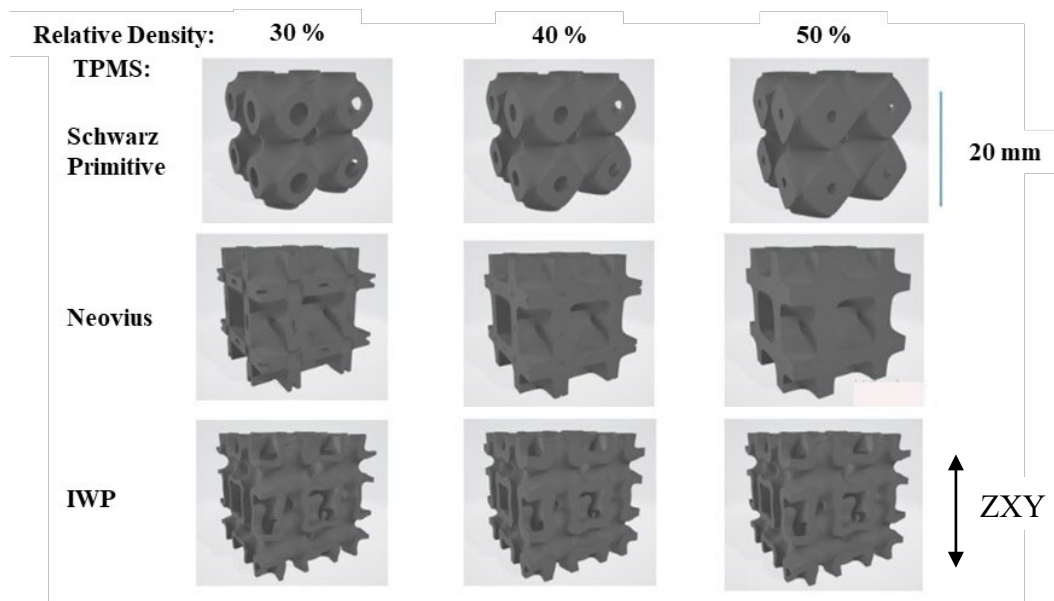


Figure 3.6 3D CAD models of Schwarz Primitive, Neovius, and IWP TPMS lattice structures designed in this study.

3.1.5 Production of TPMS Lattice Structures with Pristine Polymeric Filaments

A commercial desktop FFF machine (Bluer, Two Trees V1, China) has been utilized for the 3D printing of the designed lattice structures (TPMS) using pristine filaments in this study (Figure 3.7). Initially, as the control samples, TPMS lattice structures were fabricated using pristine PLA and PP polymers, applying the FFF process parameters given in Table 3.5.

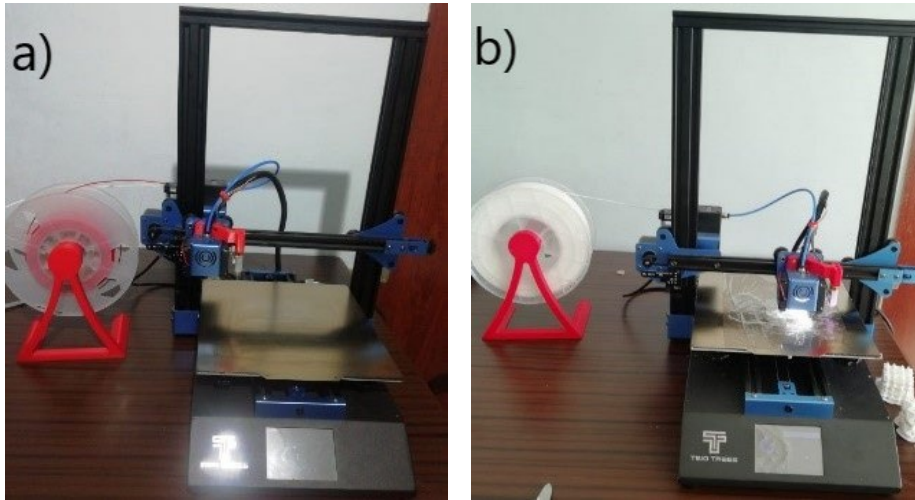


Figure 3.7 FFF process by using (a) PLA and (b) PP filaments.

Table 3.5 FFF process parameters applied for the fabrication of TPMS lattice structures using pristine PLA and PP.

Parameters	PLA	PP
Layer height (mm)	0.2	0.2
Infill (%)	100	100
Build plate temperature (°C)	60	100
Printing temperature (°C)	210	230
Printing speed (mm/s)	60	60

Pristine PLA and PP filaments 1.75 mm in diameter can be fabricated with a conventional FFF machine. PLA filament adheres easily to the printing platform. On the other hand, the printability of the PP filament is not as good as that of the PLA filament, where there is a surface detachment problem between the deposited PP and the printing platform. Therefore, to increase the adherence in the case of the PP material, the surface of the platform should be coated with sealing tape because the sealing tape is also a PP-based material, and it promotes adherence. To enhance adhesion between subsequently deposited layers and hence to optimize mechanical

properties in the applied 3D printing, a relatively small nozzle (0.4 mm in diameter) was employed to achieve minimal layer thickness.

3.1.6 Production of TPMS Lattice Structures with Metal/Polymer Composite Filaments

In this study, a commercial desktop FFF machine has also been utilized for the 3D printing of the designed lattice structures (TPMS). Metal/polymer composite filaments were used by applying the FFF process parameters given in Table 3.6. These productions were made with PLA and PP matrix composite filaments containing 5 vol% metal additives.

Table 3.6 FFF process parameters applied for the fabrication of TPMS lattice structures using metal/polymer composite filaments.

Printing Parameters	Fe/PLA Composite	Fe/PP Composite
Layer height (mm)	0.2	0.2
Infill (%)	100	100
Build plate temperature (°C)	50 (first layer) 20 (other layers)	60
Printing temperature (°C)	230	205
Printing speed (mm/s)	60	50

During the processing of the metal/polymer composite filaments via FFF there is a complication which is not present in the case of the processing with pristine polymers. This is the wear problem of the metallic nozzle with the abrasive metallic particles present in the fused polymer. Therefore, tool steel nozzles were used to process pristine polymeric filament while, ruby, which is a ceramic based nozzle, must have been chosen for the fabrication of composite filaments.

3.2 Characterization Studies

3.2.1 Sample Preparation and Examination

Composite filaments were placed in bakelite parallel and perpendicular to the surface for microstructural examination and sectioned using a precision abrasive cutter (Buehler, IsoMet 5000). The surfaces of the samples were then polished with diamond suspension from 6 to 1 μm after being ground with SiC emery papers up to 3000 grit size. After being cleaned with deionized water and ethanol, the samples were etched for 30 to 50 seconds with Nital reagent (Table 3.7). After compression testing, an optical microscope was used to take images of the TPMS lattice structures.

Table 3.7 Composition of Nital Reagent.

Etchant	Composition	Method
Nital Reagent	5 vol% HCl 95 vol% Ethanol	Immersion

3.2.2 Mechanical Characterization TPMS Lattice Structures by Compression Test

The ISO 13314:2011 standard was followed for performing the compression tests on 3 samples for every condition. On TPMS lattice structures made of pristine polymers or composite filaments, static uniaxial compression loading tests were carried out using a universal testing device, Instron 5582, with a 50 kN load cell. During the tests, the load was applied parallel to the building direction.

All TPMS specimens were pressed between hardened steel compression platens with a spherical seat to overcome any slight misalignment along the load train. The compressive strain in these tests reached up to 60% of the original specimen's length,

which is the point at which densification of the test specimen begins. The test specimens were then positioned between the test machine's moving head and stationary head. During compression testing a cross-head displacement rate of 5 mm/min was used. The average of at least three measurements has been used to compare all experimental results. The ZXY orientation, aligned with ISO/ASTM 52921-13 standard, was chosen as it offers the best mechanical performance for compression testing. This decision was made while considering the constraints of the FFF printing technique and the intricate nature of TPMS lattice structures.

The compressive offset stress, also known as compressive yield strength, is the stress level reached at the plastic compressive strain of 0.2%. Among the compressive properties, Elastic Modulus is the gradient of the straight line lying on the linear deformation region at the beginning of the curve.

There are different approaches in the literature for cross sectional area in the calculation of nominal stress. In one study, the cross section of lattice parts, which are produced with pristine PLA and PP, is 1600 mm², assuming that the part is solid in dimensions of 40x40x40 mm. The cross section of the lattice part, which is produced with composite PLA and PP as 400 mm², assumes that the part is solid in dimensions of 20x20x20 mm [36]. On the other hand, the average of the maximum and minimum cross sectional areas was used in another study to consider the effect of the varying cross sections through the lattice [37]. In Figure 3.8, minimum and maximum cross section area of 30% relative density Schwarz Primitive. In the current study, the average cross sectional area approach has been used for the nominal stress calculation, and the average cross sectional areas for each topology are shown in Table 3.8.

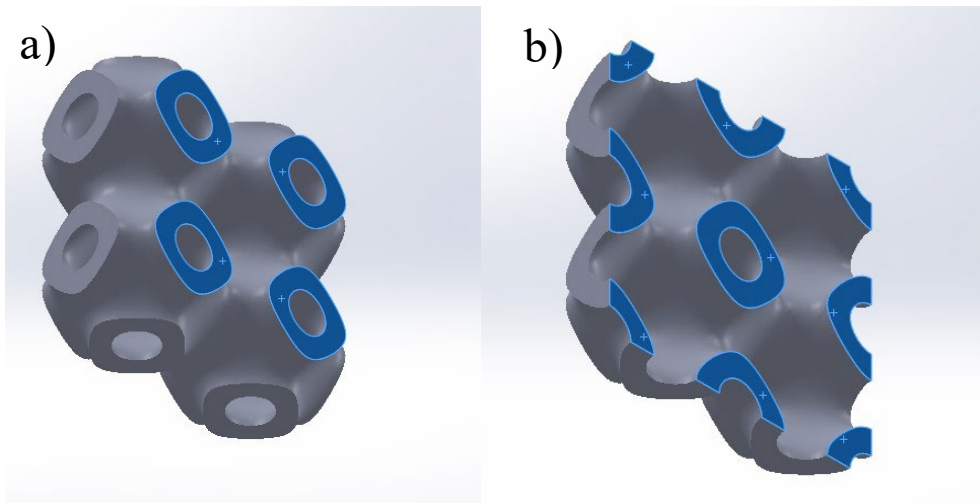


Figure 3.8 (a) Minimum and (b) maximum cross sectional area of the Schwarz Primitive TPMS structure with 30% relative density.

Table 3.8 Average cross section area for each TPMS used in compression tests.

TPMS Material	Schwarz Primitive Cross Section Area (mm ²)			Neovius Cross Section Area (mm ²)			IWP Cross Section Area (mm ²)		
	30%	40%	50%	30%	40%	50%	30%	40%	50%
Pristine PLA/PP	381	511	663	457	609	762	341	445	576
Composite PLA/PP	95	127	163	114	152	190	85	111	144

3.2.3 Calculation of Mechanical Properties with Rule of Mixture Method

The rule of mixture method calculates the upper and lower limit for homogeneously distributed large particle reinforced composite materials. Mechanical property range can be calculated by using the components' volume ratio and mechanical properties according to equation 3.4 and equation 3.5 [34],

$$E_c(u) = E_m V_m + E_p V_p \quad (\text{Eqn. 3.4})$$

$$Ec(l) = \frac{EmVp}{VmEp + VpEm} \quad (Eqn. 3.5)$$

where $Ec(u)$ is the upper mechanical limit for composite, $Ec(l)$ is the lower limit for the mechanical properties of the composite, Em is the mechanical property of the matrix material, Ep is the mechanical property of the particle or reinforcement; Vm is the volume fraction of the matrix material, and Vp is the volume fraction of the particle.

The volume fraction of the components for three batches is given in Table 3.9. Stearic acid composition is neglected because the ratio is insignificant, and there is no contribution to the mechanical properties of the composite filaments. The mechanical properties of the components are shown in Table 3.10.

Table 3.9 Volume fraction of composite filaments.

Filament	Fe ratio	TPU ratio	PP ratio	PLA ratio	Stearic Acid ratio
Batch 1	0.30	0.09	0.58	-	-
Batch 2	0.05	0.03	0.91	-	-
Batch 3	0.05	0.03	-	0.91	-

Table 3.10 Mechanical properties of the components.

Component	Elastic Modulus (MPa)	Compressive Yield Strength (MPa)
Fe	204000-212000	110-220
TPU	7.2	5-6
PP	1670	40
PLA	3500	65

3.2.4 Microstructural Characterization

An optical microscope (Nikon, Otiplot-100, Japan) was used to take cross sectional images of composite filaments. Additionally, it was also used to analyze the fractured surfaces after the compression tests.

Using a scanning electron microscope (SEM) (Nova NanoSEM 430, FEI Company, Eindhoven, the Netherlands) run at 5-18 kV accelerating voltage, the morphology of the metallic particles was observed. SEM images were used to determine the dimensions of the powders to compare them with the results of the particle size analyses. The SEM's energy dispersive spectroscopy (EDS) detector was also used to evaluate the chemical composition of the samples.

3.2.5 Simulation of the Mechanical Behavior of TPMS Lattice Structures Through Finite Element Analysis

A finite element model (FEM) was constructed to characterize the stress-strain response of 3D-printed TPMS lattice structures. It is essential to highlight that these structures' Finite Element Analysis (FEA) was primarily directed at the elastic portion of the stress-strain curve, encompassing parameters such as the elastic modulus and yield strength. The deformation characteristics of the IWP lattice structure were simulated using the Ansys program. Based on the outcomes of the compressive tests, the IWP model emerges as the most favorable among the various models with respect to mechanical performance. Consequently, the modeling section is centered around a comprehensive analysis of the IWP, aiming to delve deeper into its mechanical characteristics.

Mechanical data obtained from the real compression tests of the fully dense cubes produced with pristine PP filament and known material properties of PP (density, Poisson's ratio) were provided as program input for TPMS design compression testing. In a second modeling approach, cubes manufactured with metal particle incorporated PP matrix composite filaments were used, and the mechanical data (e.g.

Compressive elastic modulus) obtained from the real compression tests of these cubes were presented as program input. On the other hand, the reinforced PP's material properties such as density and Poisson's ratio were calculated using the rule of mixtures.

In the FEM simulations of compression samples, due to the absence of validated data containing essential coefficients for defining damage mechanisms, investigations were conducted by subjecting the samples to loads up to a 3 mm/mm strain level. This aligns with the point at which the samples approach to their initial maximum compressive stress. It was determined that a 0.25 mm average element size would be sufficient to produce computed replies with a reasonable level of accuracy.

In Table 3.11, the basic mechanical properties of 5 vol% Fe/PP composite material are given. These values were used as material property input for FEM analysis.

Table 3.11 Basic properties of the 5 vol% Fe/PP composite from compression test and rule of mixture.

Material Property	Value
Density (g/cm ³)	1.29
Elastic modulus (MPa)	320
Poisson ratio	0.42

In the modeling, the speed of upper cross-head movement was increased much more than the experimental compression test (5 mm/min) without producing incorrect results in the explicit time integration to reduce calculation time. Even though the experimental maximum displacement was significantly larger and corresponded to half of the height of the compressed IWP models, the maximum cross-head displacement that marked the end of the simulation in the case of static tests was 12 mm for all simulations of IWP specimens 20 mm in height. However, as the compression test progressed, it was not possible to produce meaningful data. Therefore, the data used in the modeling mechanical value graphs were taken before the 3 mm/mm stain value.

CHAPTER 4

RESULT AND DISCUSSION

4.1 Microstructural Examination

4.1.1 Metal Powder

After sieve analysis, iron powder was examined via SEM to observe the morphology and size of the powders used. The size and morphology of the particles play an important role in determining the mechanical properties and quality of composite filaments to obtain elastic behavior and good printing quality. As shown in Figure 4.1, the Fe particles have plate-like morphology.

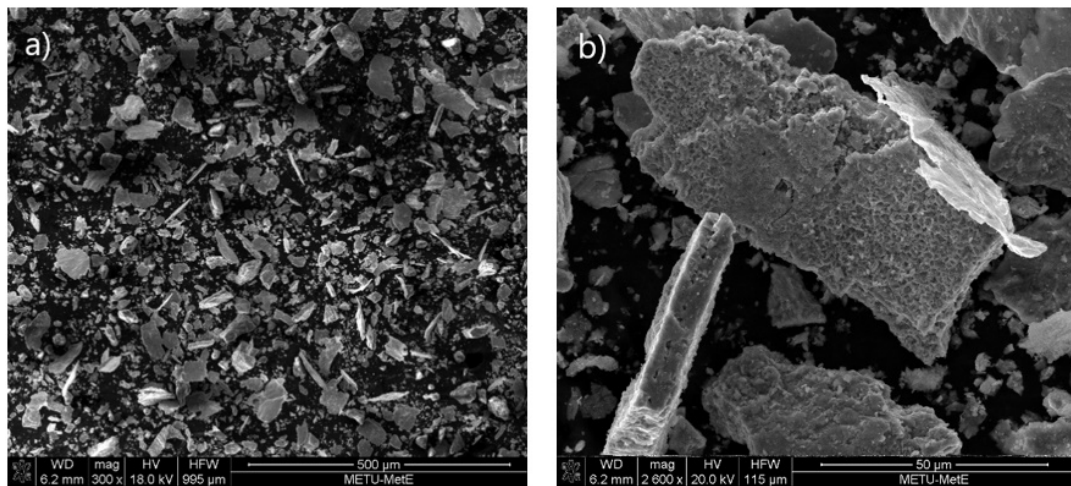


Figure 4.1 SEM images of sieved Fe powders at (a) lower and (b) higher magnification.

Although the expectation was to have Fe powders with spherical morphology because they were produced with gas atomization, SEM images (Figure 4.1) of the

sieved powders show that they have plate-like morphology. This discrepancy should be related to the aspect ratio of the powders. Particles that are longer than their width must have passed through the sieve. However, spherical powders bigger than $53\ \mu\text{m}$ could not pass through the sieve, as seen in (Figure 4.2). Powders with plate-like morphology can behave as a stress concentrator or crack nucleation site and hence may lead to a brittle composite filament behavior.

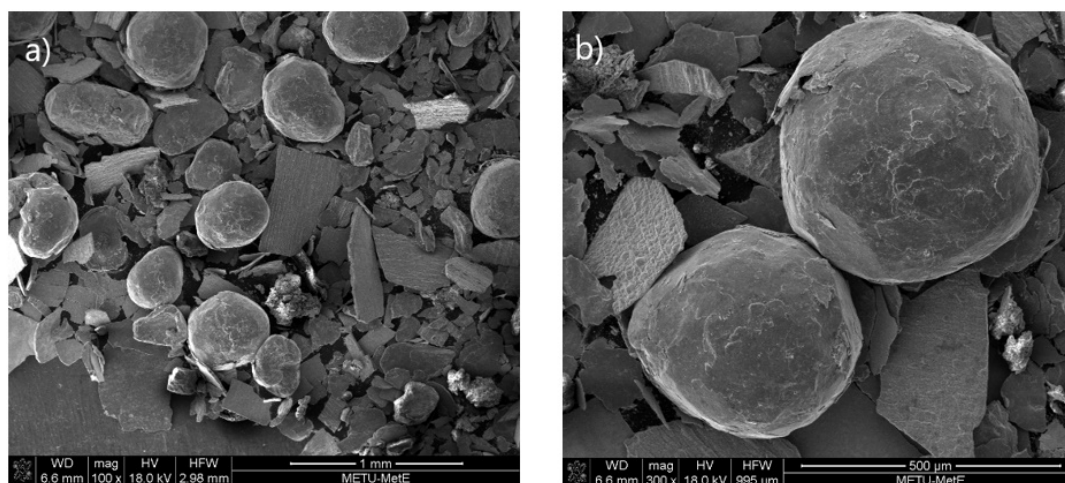


Figure 4.2 SEM images of not sieved Fe powders at (a) lower and (b) higher magnification.

4.1.2 Composite Filament

The Fe particles should be evenly distributed and disseminated throughout the filament, which is a distinctive feature of the feedstock filaments. The cross sectional cut of a filament shown in Figure 4.3 makes it clear that the metal particles are evenly distributed throughout the 30.8 vol% iron containing PP matrix composite filament. For 5 vol% iron containing PP matrix composite filaments, a similar powder dispersion was observed (Figure 4.4). For the proper 3D printing process, adequate particle dispersion and distribution must exist in the filaments. As seen in Figure 4.5, a few small cavities and porosity are visible in 5 vol% iron containing PLA matrix composite filaments. These filaments were still printable, even though they had defects such as pores $\sim 200\ \mu\text{m}$ in maximum size and agglomerates $\sim 50\text{-}200\ \mu\text{m}$ in size (Figure 4.5).

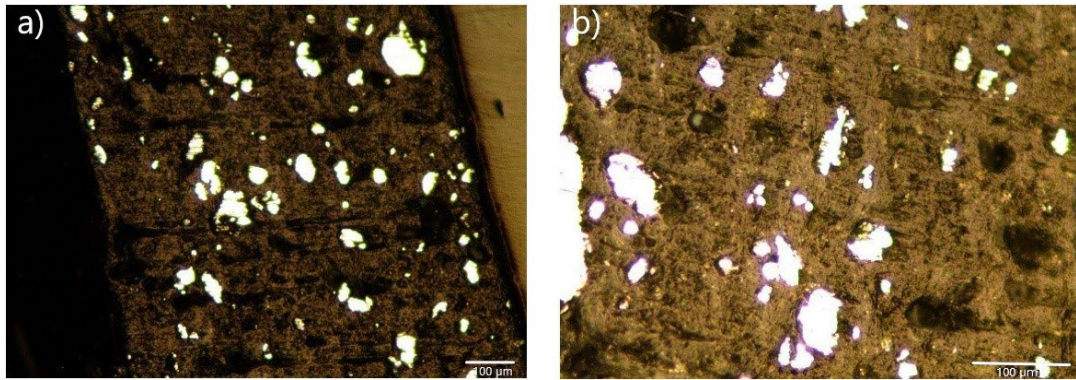


Figure 4.3 Cross sectional view of PP matrix composite filament with 30.8 vol% iron particles (a) horizontal and (b) vertical section.

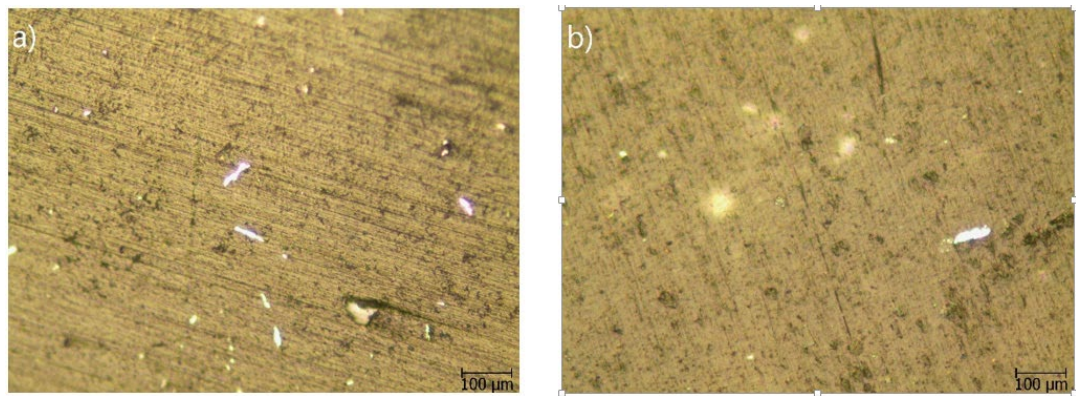


Figure 4.4 Cross sectional view of PP matrix composite filament with 5 vol% iron particles (a) horizontal and (b) vertical section.

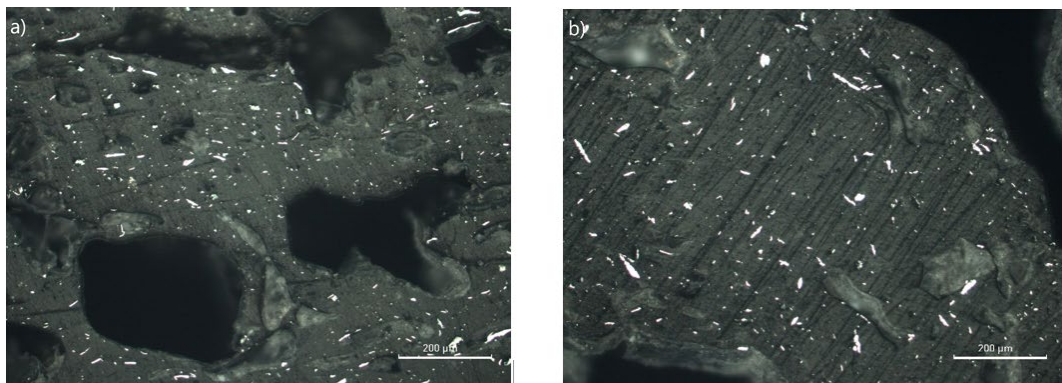


Figure 4.5 Cross sectional view of PLA matrix composite filament with 5 vol% iron particles (a) horizontal and (b) vertical section.

4.2 Bulk Specimens Produced with FFF

4.2.1 Fully Dense Cubic Specimens

Cubic specimens were produced using pristine PLA, PP, and composite filaments. In the case of the fully dense cubes 3D printed using composite filaments, the produced material retained the same particle distribution and dispersion as that seen in the filament. Figure 4.6 depicts an optical microscope view of a 3D printed cube surface created using metal particle-containing filaments. The sample produced with the composite filament containing 30.8 vol% metal particles (Figure 4.6a) has a more porous structure than the one produced with the composite filament containing 5 vol% particles (Figure 4.6b). Additionally, as the number of metal particles increases, it becomes more difficult to distinguish between the layers of the 3D printed structure.

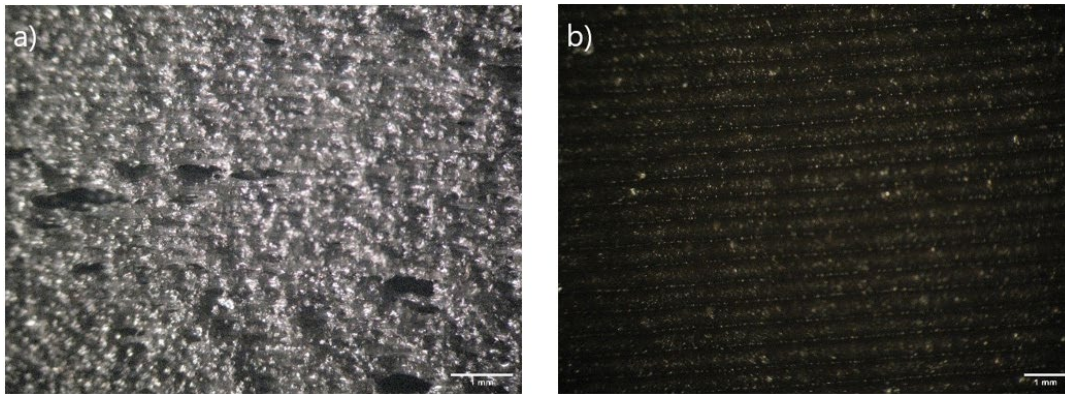


Figure 4.6 Printing surface of the bulk specimens made of PP matrix composite filaments filled with (a) 30.8 vol% and (b) 5 vol% iron particles.

4.2.2 Compressive Test Results of Bulk Specimens

Compressive tests were applied on fully dense bulk specimens to obtain the material properties of additively manufactured pristine polymers and composite structures. The results of the compressive tests of the cubic specimens are summarized in Table 4.1. Average values of 3 measurements are presented together with \pm standard deviations. Mechanical properties of the bulk specimens calculated using the rule of mixtures based on the volumetric contents and reported inherent material properties of the composite constituents are also given in Table 4.1. According to Table 4.1, pristine PLA has a higher compressive strength value than pristine PP in fully dense cubic form. This result is expected due to the nature and material strength of these polymers. The addition of the reinforcing particles seems to have deteriorated the mechanical properties of the PLA matrix. The PLA matrix seems unsuitable for reinforcement; reinforcing the PLA matrix does not cause an increase in mechanical properties due to weak interfacial bonding between PLA and metallic particles. In addition, weak bonding at the interface may have resulted in the defects such as pore existing in the composite filament (Figure 4.5)) deteriorate the mechanical properties of the PLA. Air gaps in the PLA matrix composite cause deviation and deterioration in the strength values of the produced cubic structure. On the other hand, it is seen that compressive elastic modulus and stress values increase as the amount of additive increases for PP matrix. This result is expected according to the rule of mixture. PP based matrix mixture seems more suitable for particle reinforcements.

Table 4.1 Compressive test results of the bulk specimens.

Mechanical Properties	Compressive Elastic Modulus (MPa)	Compressive Yield Strength (MPa)	Maximum Compressive Stress (MPa)
Material			
Pristine PLA	2275 ± 12.17	86.0 ± 0.87	181 ± 4.28
Pristine PP	292.5 ± 21.62	-	64.5 ± 3.40
5 vol% Fe/PLA	227.4 ± 13.42	-	77.6 ± 1.89
5 vol% Fe/PP	320.6 ± 52.57	-	68.1 ± 9.46
30.8 vol% Fe/PP	535.5 ± 155.0	6.60	84.3 ± 8.6
5 vol% Fe/PLA (Rule of mixture)	13420.2	68.2	-
5 vol% Fe/PP (Rule of mixture)	11736.6	45.2	-
30.8 vol% Fe/PP (Rule of mixture)	62185.2	72.5	-

4.3 Lattice Structure Specimens Produced with FFF

4.3.1 TPMS Lattice Structure Specimens

TPMS lattice structures, which are Schwarz primitive, Neovius, and IWP were produced with FFF methods. Four different filaments which are pristine PLA and pristine PP along with 5 vol% iron particle containing PLA and PP matrix composite filaments were used for the 3D-printed TPMS lattice structures. In the case of pristine filaments, all of the three studied TPMS lattice structures with three different relative densities of 30%, 40% and 50% were successfully produced as shown in Figure 4.7.

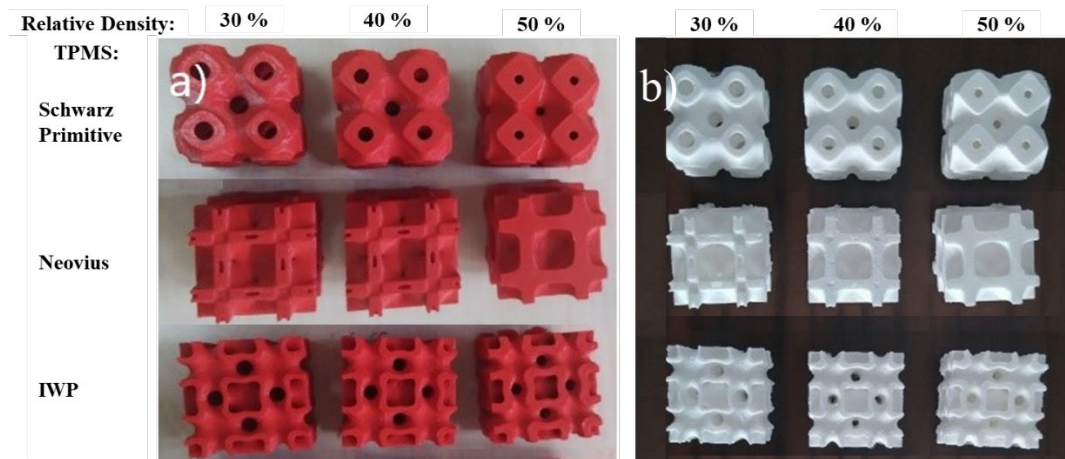


Figure 4.7 3D-Printed TPMS lattice structures (a) PLA and (b) PP specimens with different relative densities.

3D printing of selected lattice structures using 5 vol% metal particle containing composite filaments with PLA and PP matrices was also conducted. A relatively low amount of particle incorporation (5 vol%) with a suitable particle size and size distribution has led to proper filament production and 3D printing of lattice models as shown in Figure 4.8 and Figure 4.9. On the other hand, TPMS models with particle contents higher than 5 vol% could not be produced with the FFF method. The high density of the metallic particles in the polymeric matrix has led to the flow down of the composite filament during the processing of the lattice structures. Another side effect of the high volume percent of metallic particles, which is generally 50-100 μm in size, is decreasing the manufacturability of the composite filament. When particle content increases, producing composite filament with homogenous diameter size becomes hard. Therefore, inhomogeneous distribution of the filament diameter can block up the nozzle. Consequently, even though 30.8 vol% Fe particle containing PP matrix composite filament could have been used for the 3D printing of the fully dense cube specimens, the same filament could not be used for the printing of lattice structures.

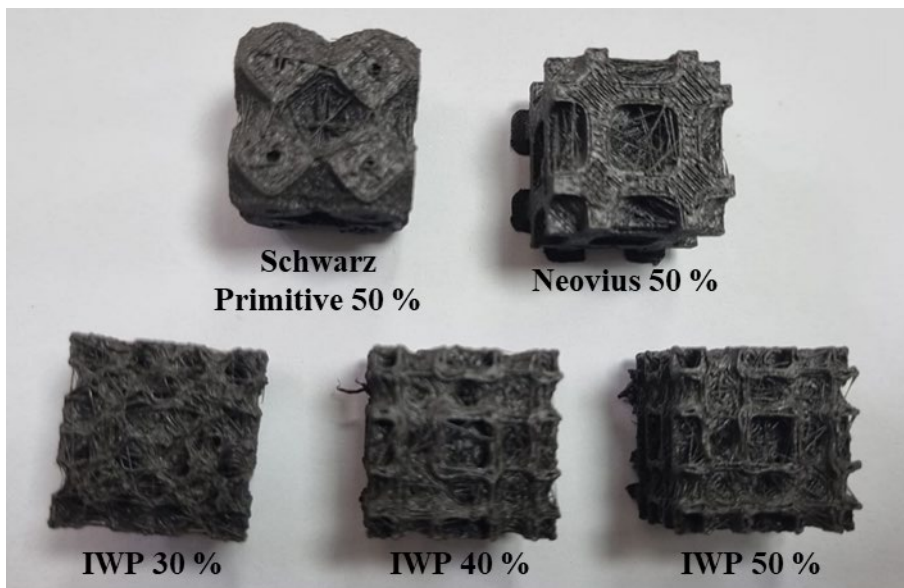


Figure 4.8 Selected TPMS lattice structure specimens 3D printed using 5 vol% Fe/PLA composite filaments.

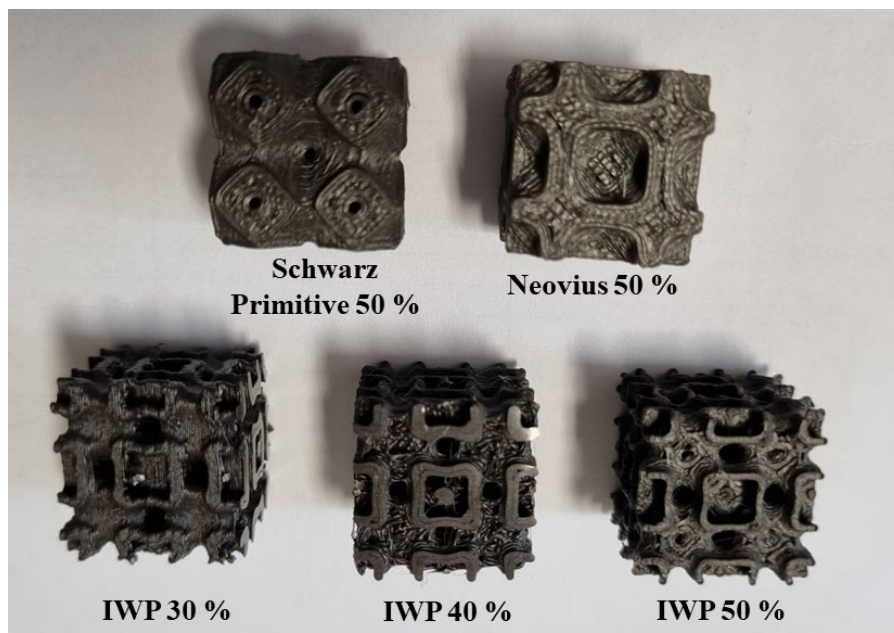


Figure 4.9 Selected TPMS lattice structure specimens 3D printed using 5 vol% Fe/PP composite filaments.

4.3.2 Fracture Surface Analyses of Compression Tested TPMS Lattice Structures

After the compression tests, optical microscope analysis was done on the fracture surface of the tested lattice structures. Fracture surface images for pristine PLA and PP lattice structures with 30% relative density are shown in Figure 4.100 and Figure 4.111, respectively. The Schwarz Primitive structure shows intense shearing events resulting in material fracture at the middle section of the specimen. Neovius and IWP structures do not show similar fracture behavior with Schwarz Primitive structure under the same amount of straining. Therefore, it can be concluded that the load transfer mechanism works more successfully in Neovius and IWP geometries compared to Schwarz Primitive models under compressive stress.

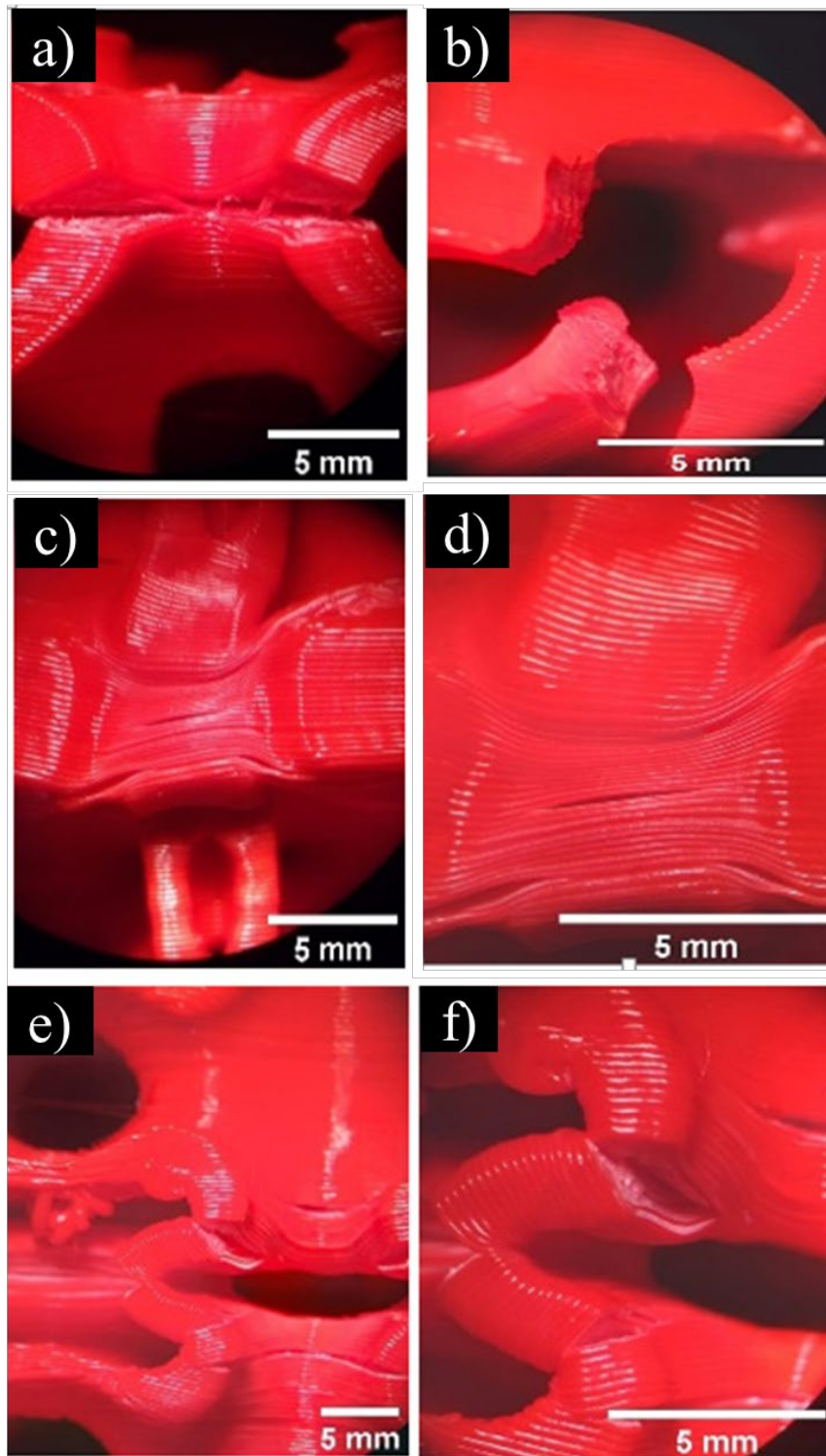


Figure 4.10 Fracture surfaces of TPMS lattice structures 3D printed using pristine PLA and compression tested at 15% strain (a, b) Schwarz Primitive, (c, d) Neovius and (e, f) IWP with 30% relative density.

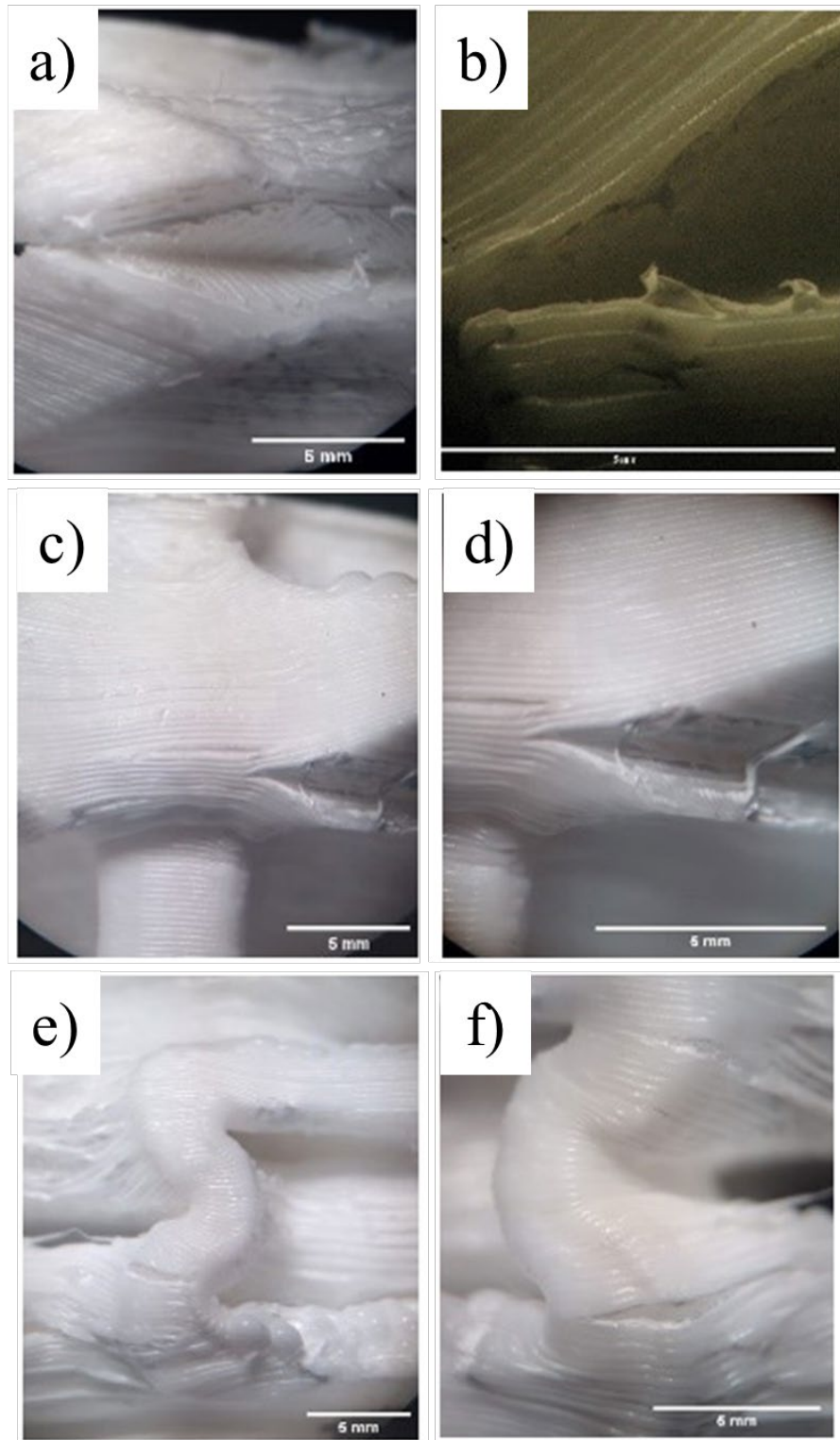


Figure 4.11 Fracture surfaces of TPMS lattice structures 3D printed using pristine PP and compression tested at 15% strain (a, b) Schwarz Primitive, (c, d) Neovius and (e, f) IWP with 30% relative density.

In Figure 4.122, fracture surface of the compression tested TPMS lattice structure 3D printed using 5 vol% particle containing PLA matrix composite filament is shown. According to these images, there seems to be detachment between layers. (Figure 4.122). This must have led to delamination between the layers which is detrimental to the mechanical properties of the lattice structures made of 5 vol% Fe/PLA composite filament.

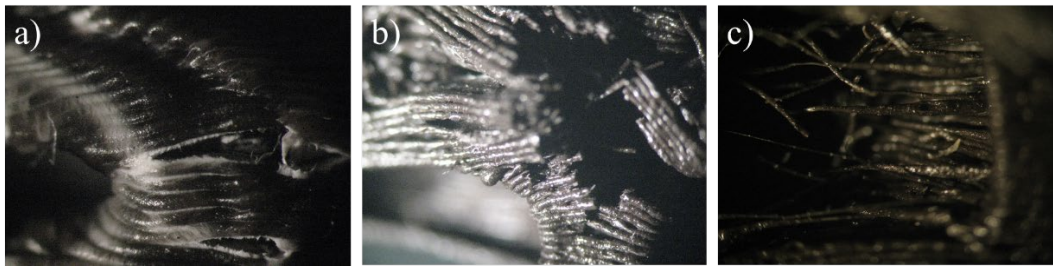


Figure 4.12 Fracture surfaces of TPMS lattice structures 3D printed using 5 vol% Fe/PLA composite filaments compression tested at 15% strain (a) Schwarz Primitive, (b) Neovius, and (c) IWP.

Figure 4.13 shows the compression tested fracture surface of the TPMS lattice structure 3D printed using 5 vol% particles containing PP matrix composite filament. Different than metallic particle containing PLA filament, PP matrix composite filament has led to the formation of less additive manufacturing defects such as air gap and nonuniformity in the cross section. As a result, the mechanical performance of the TPMS lattice structures 3D printed using 5 vol% Fe/PP composite filaments has the potential to approach to the expected levels.

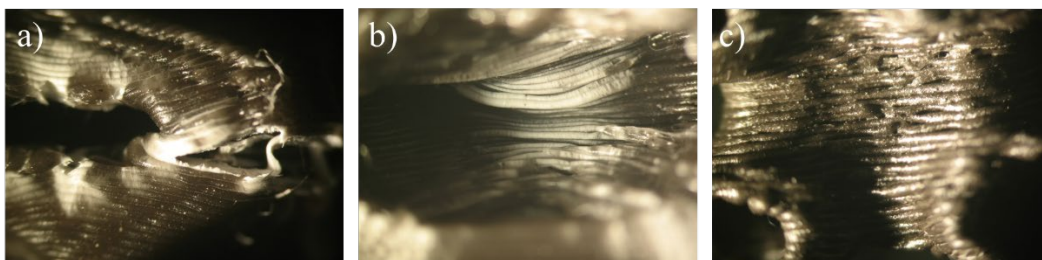


Figure 4.13 Fracture surfaces of TPMS lattice structures 3D printed using 5 vol% Fe/PP composite filaments compression tested at 15% strain (a) Schwarz Primitive, (b) Neovius, and (c) IWP.

4.3.3 Mechanical Properties of the TPMS Lattice Structures

Figure 4.144 and Figure 4.155 show how each TPMS structure deformed in response to the applied compressive stress. Additionally, it displays the state of each structure for various strains (0%, 5%, and 10%). As observed in this sequence, rigidity of the lattice structures increases from Schwarz Primitive to Neovius and IWP for all relative densities at all strain levels. As shown in Figure 4.144 and Figure 4.155, different than Schwarz Primitive and IWP, Neovius structure did not collapse at any of the strain levels showing that it has the highest structural load bearing capability.

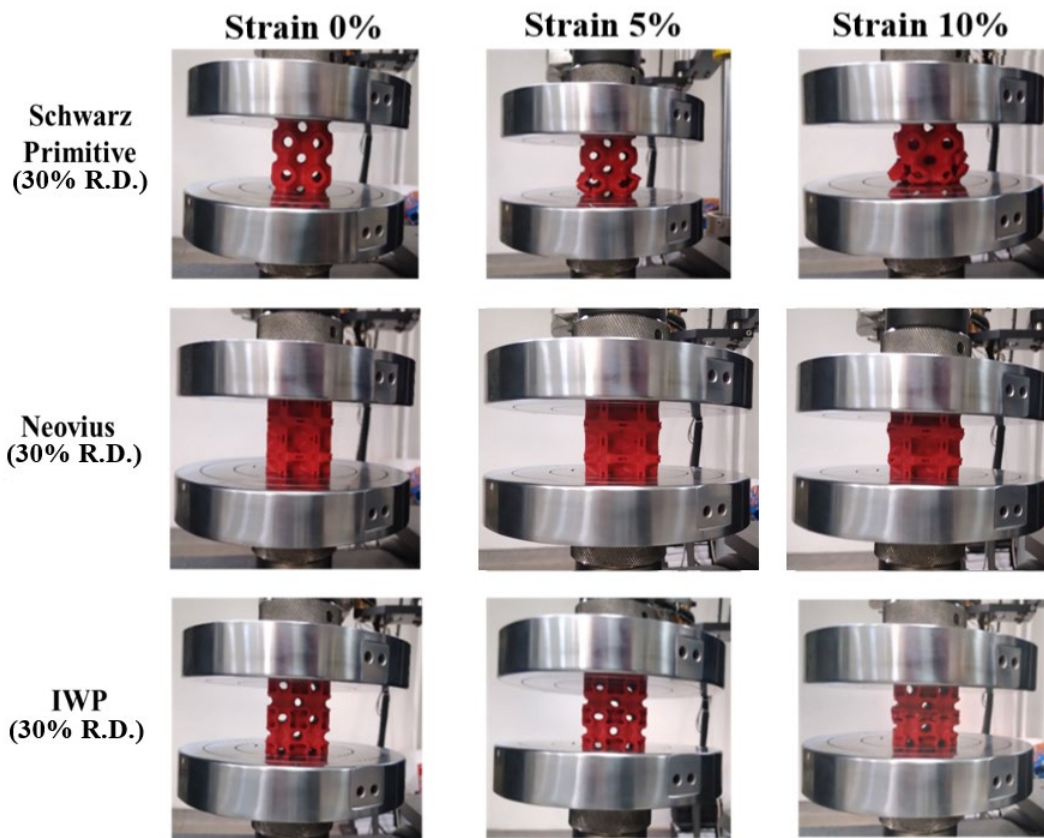


Figure 4.14 Deformation frames of Schwarz Primitive, Neovius, and IWP lattice structures 3D printed using pristine PLA at 0%, 5%, and 10% strain.

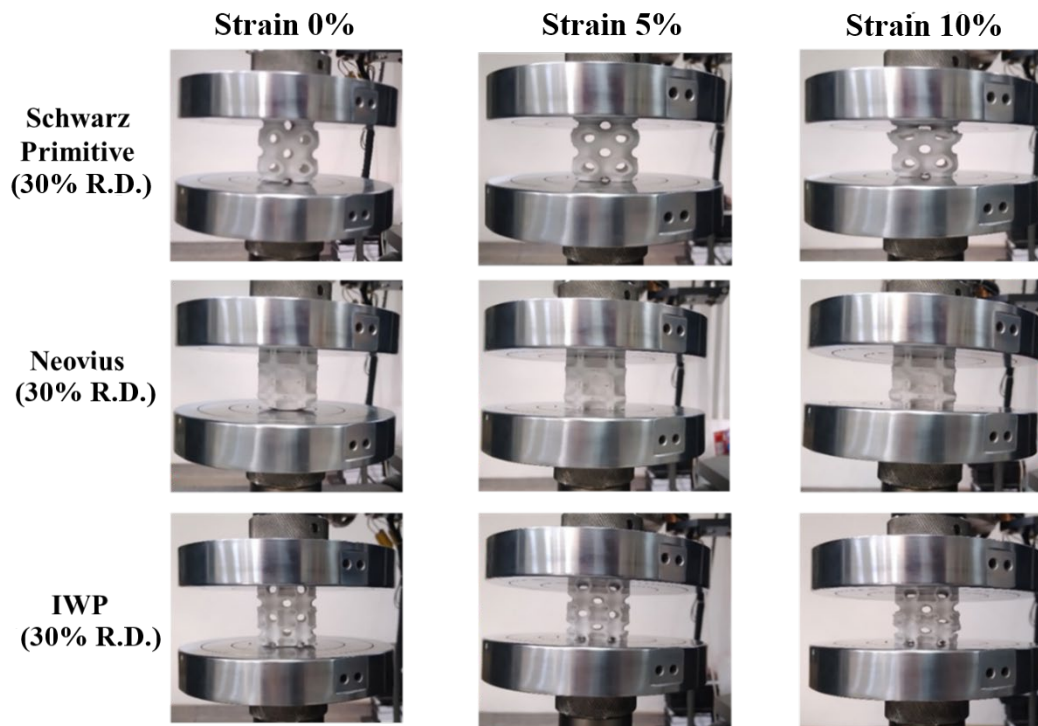


Figure 4.15 Deformation frames of Schwarz Primitive, Neovius, and IWP lattice structures 3D printed using pristine PP at 0%, 5%, and 10% strain.

Figure 4.16 shows compressive force-displacement curves for compression testing on pristine PLA and PP TPMS specimens manufactured using 3D printing technology. Figure 4.17 and show the compressive force-displacement curves of the TPMS structure which was produced with 5 vol% metal containing PLA and PP matrix composite filaments, respectively. According to these curves, it is observed that as relative density increases, compressive force values generally increase. In addition, the structures produced with the IWP design resisted greater compressive loads compared to other models. IWP lattices have higher compressive strength value thanks to their load bearing capability.

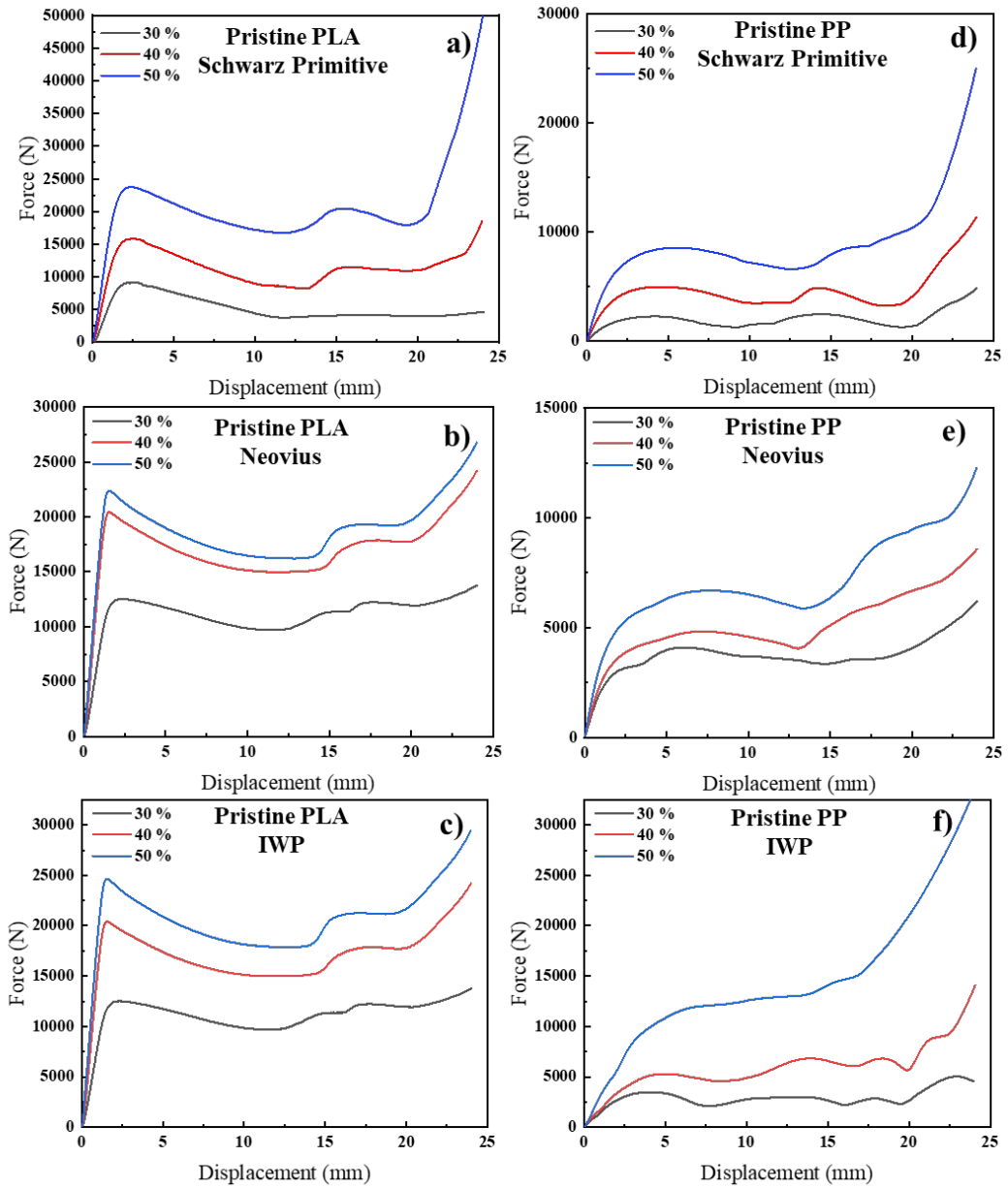


Figure 4.16 Compressive force-displacement curves of pristine (a) PLA Schwarz Primitive, (b) PLA Neovius, (c) PLA IWP; (d) PP Schwarz Primitive, (e) PP Neovius, (f) PP IWP structures.

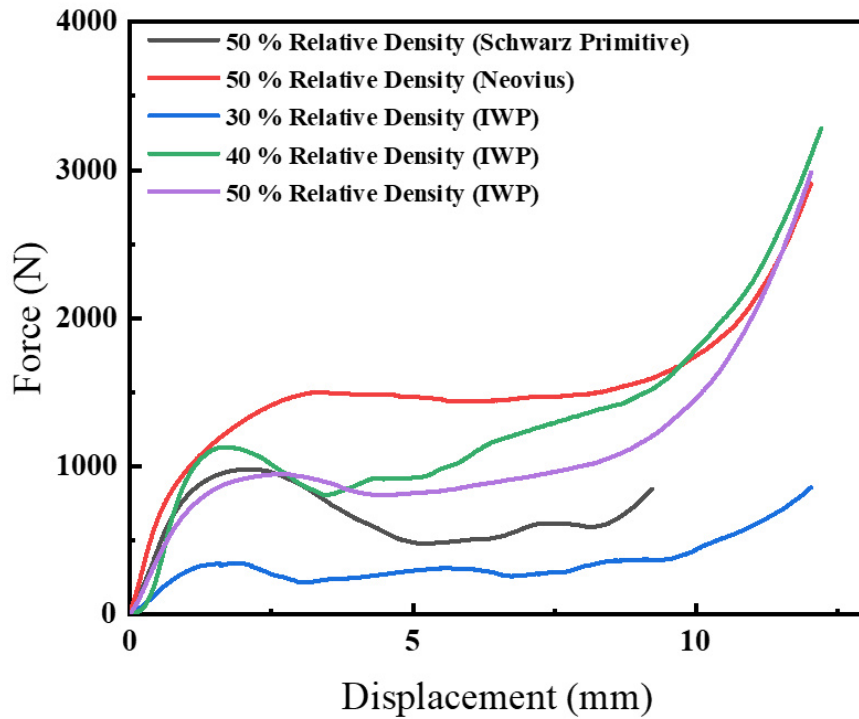


Figure 4.17 Compressive force-displacement curves of 5 vol% Fe/PLA TPMS.

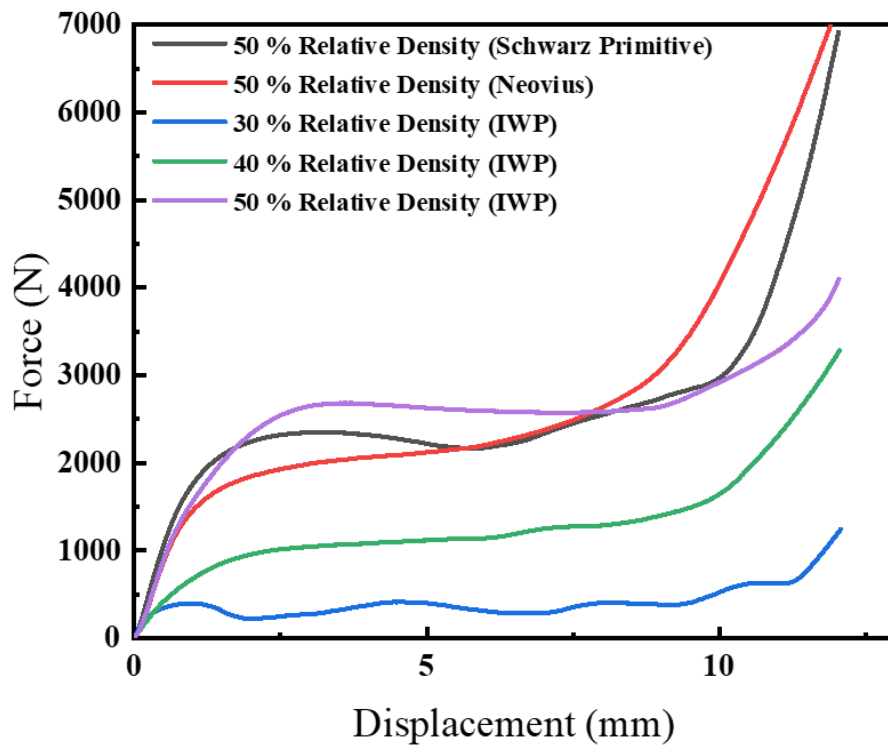


Figure 4.18 Compressive force-displacement curves of 5 vol% Fe/PP TPMS.

The findings of the compression tests of TPMS lattice structures 3D printed using pristine as well as composite filaments are tabulated in Table 4.2 - Table 4.5. Table 4.2 shows compressive test results of TPMS lattice structures made of pristine PLA.

Table 4.3 shows compressive test results of TPMS lattice structures made of pristine PP. Compared to Schwarz Primitive and Neovius structures, IWP structures, which are made from pristine PLA and PP, have higher mechanical values such as compressive elastic modulus and compressive yield strength. According to Table 4.2, it can be said that IWP (50% relative density) had the highest yield stress with 44.2 MPa and elastic modulus with 1629 MPa while Schwarz Primitive (50% relative density) and Neovius (50% relative density) have yielded at lower stress levels (31 MPa and 24.8 MPa, respectively). In addition, it is observed that higher relative density generally leads to higher compressive maximum stress and yield strength for pristine PLA and PP structures, as shown in Table 4.2 and

Table 4.3. In addition, Schwarz Primitive, Neovius and IWP structures with 50% relative density and all IWP specimens having 30%, 40%, and 50% relative density are promising designs for compressive loading. Any reason that leads to fast cooling during FFF processing may lead to insufficient melting. Consequently, some of the TPMS structures made of pristine PP do not show yield points (Table 4.3) revealing brittle behavior. It may be related to the processing of the PP filament and its high sensitivity to atmospheric conditions.

Table 4.4 shows compressive test results of TPMS lattice structures made of 5 vol% Fe /PLA composite filaments. According to this table, an increase in relative density leads to compressive load resistance of the IWP specimens. On the other hand, there is no notable difference between the mechanical values of the Schwarz Primitive, Neovius and IWP structures with 50% relative density. The absence of a notable enhancement in mechanical properties across the models could be linked to the inadequacy of the particle incorporated PLA filament's quality for FFF purposes, as well as discontinuity in additive manufacturing processes. These additive manufacturing discontinuities may be detachment between layers, air gaps, and

voids. Detachment and delamination problems are pronounced in TPMS structures made of 5% Fe/PLA filament.

Table 4.5 shows compressive test results of TPMS lattice structures made of 5 vol% Fe/PP composite filaments. When the compressive test results of PP matrix composite filaments are compared, it is seen that IWP (50% relative density) had the highest yield stress with 17.36 MPa, while Schwarz Primitive (50% relative density) and Neovius (50% relative density) have yielded at lower stress levels (14.5 MPa and 13.8 MPa, respectively). Different from PLA matrix composite filament, there is some increase in mechanical values such as compressive yield stress and maximum compressive stress for all specimens of PP matrix composite owing to reinforcements. In this case, it has been observed that PP material is more suitable for strengthening with additives and for additive manufacturing compared to PLA, which contains the same amount of components and additives.

Upon increasing relative density from 30% to 50%, lattice models generally show higher strength and elastic modulus values. This is expected because with increasing density, the wall thicknesses in the lattice structures get wider providing higher compressive load bearing capability. On the other hand, the IWP model shows relatively higher maximum compressive stress and yield strength values compared to Neovius and Schwarz Primitive structures. It may arise from the design of IWP, which leads to effective stress distribution. In addition, IWP has a self-supported structure. However, Neovius and Schwarz Primitive models have wider lattice gaps inside, where unsupported gaps can cause detachment between layers.

Table 4.2 Compressive test results of TPMS lattice structures made of pristine PLA.

Mechanical Properties	Compressive Elastic Modulus (MPa)	Compressive Yield Strength (MPa)	Maximum Compressive Stress (MPa)
Material			
Schwarz Primitive ($\rho=30\%$)	768.6 \pm 19.3	20.5 \pm 1.2	25.2 \pm 0.5
Schwarz Primitive ($\rho=40\%$)	851.3 \pm 21.6	22.5 \pm 1.5	82.9 \pm 1.87
Schwarz Primitive ($\rho=50\%$)	1098.9 \pm 60.0	31.0 \pm 3.3	44.8 \pm 8.2
Neovius ($\rho=30\%$)	940.1 \pm 71.7	31.8 \pm 5.6	38.1 \pm 17.8
Neovius ($\rho=40\%$)	968.2 \pm 40.3	26.2 \pm 8.6	29.1 \pm 10.1
Neovius ($\rho=50\%$)	1088.6 \pm 57.5	24.8 \pm 4.6	31.4 \pm 8.4
IWP ($\rho=30\%$)	1189.0 \pm 23.1	24.9 \pm 6.5	48.4 \pm 5.4
IWP ($\rho=40\%$)	1332.2 \pm 49.2	34.2 \pm 5.0	78.8 \pm 9.6
IWP ($\rho=50\%$)	1629.0 \pm 42.5	44.2 \pm 1.9	88.2 \pm 12.0

Table 4.3 Compressive test results of TPMS lattice structures made of pristine PP.

Mechanical Properties	Compressive Elastic Modulus (MPa)	Compressive Yield Strength (MPa)	Maximum Compressive Stress (MPa)
Material			
Schwarz Primitive ($\rho=30\%$)	139.3 \pm 12.8	5.0 \pm 1.6	10.8 \pm 1.7
Schwarz Primitive ($\rho=40\%$)	234.1 \pm 21.9	6.0 \pm 1.03	14.8 \pm 6.6
Schwarz Primitive ($\rho=50\%$)	265.3 \pm 6.7	8.4 \pm 0.9	22.6 \pm 12.2
Neovius ($\rho=30\%$)	211.7 \pm 31.1	5.7 \pm 1.3	15.9 \pm 4.4
Neovius ($\rho=40\%$)	207.8 \pm 74.8	4.5 \pm 0	11.2 \pm 4.2
Neovius ($\rho=50\%$)	203.8 \pm 48.5	7.08 \pm 0	11.0 \pm 4.4
IWP ($\rho=30\%$)	210.8 \pm 17.1	9.0 \pm 1.5	22.2 \pm 9.9
IWP ($\rho=40\%$)	228.5 \pm 57.6	10.9 \pm 3.6	25.4 \pm 5.4
IWP ($\rho=50\%$)	370.3 \pm 35.2	14.0 \pm 5.6	34.8 \pm 7.3

Table 4.4 Compressive test results of TPMS lattice structures made of 5 vol% Fe /PLA) composite filaments.

Mechanical Properties	Compressive Elastic Modulus (MPa)	Compressive Yield Strength (MPa)	Maximum Compressive Stress (MPa)
Material			
Schwarz Primitive ($\rho=50\%$)	138.8 ± 30.6	5.7 ± 1.3	12.3 ± 9.7
Neovius ($\rho=50\%$)	136.1 ± 20.8	5.2 ± 0.8	11.4 ± 2.8
IWP ($\rho=30\%$)	92.3 ± 37.1	3.3 ± 0.4	6.8 ± 2.9
IWP ($\rho=40\%$)	190.2 ± 82.4	6.4 ± 0.8	17.9 ± 4.9
IWP ($\rho=50\%$)	176.5 ± 63.2	5.9 ± 1.9	16.5 ± 4.5

Table 4.5 Compressive test results of TPMS lattice structures made of 5 vol% Fe /PP) composite filaments.

Mechanical Properties	Compressive Elastic Modulus (MPa)	Compressive Yield Strength (MPa)	Maximum Compressive Stress (MPa)
Material			
IWP ($\rho=30\%$)	235.5 ± 33.3	3.52 ± 1.45	9.7 ± 4.3
IWP ($\rho=40\%$)	175.7 ± 69.8	7.27 ± 0	21.9 ± 6.6
IWP ($\rho=50\%$)	161.28 ± 56.7	17.36 ± 4.4	35.42 ± 4.8
Schwarz Primitive ($\rho=50\%$)	257.8 ± 13.1	14.5 ± 0.3	26.3 ± 13.2
Neovius ($\rho=50\%$)	196.3 ± 16.2	13.8 ± 0.4	17.6 ± 2.5

4.4 Modeling of the Compression Behavior of the TPMS Lattice Structures

The uniaxial compression behavior of the IWP lattice structure has been analyzed by finite element modeling (FEM) using Ansys for comparison with the experimental data. Figure 4.19 shows a compressive stress-strain graph of Pristine PP IWP (40% relative density). According to this graph, the compressive yield strength of the Pristine PP with 40% relative density is nearly 40 MPa.

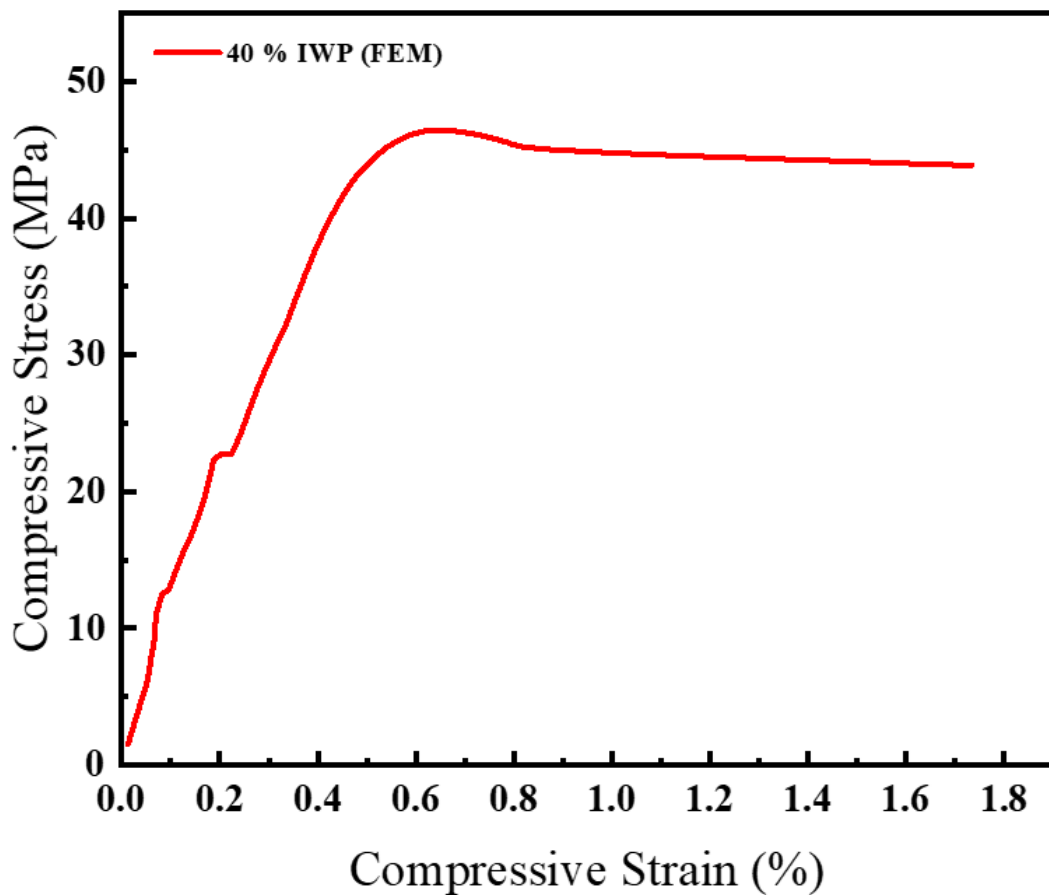


Figure 4.19 Simulated compressive stress-strain graph of Pristine PP IWP (40% relative density).

Figure 4.20 shows simulated compressive stress-strain graphs of 5 vol%/PP IWP with 30%, 40% and 50% relative density. Analyzing the FEM compression test outcomes for IWP (40% relative density) referring to graphs 4.19 and 4.20, it can be anticipated that the incorporation of metal powders into the PP matrix can lead to a noticeable increase in its mechanical properties. Nevertheless, despite the increase in the elastic modulus and maximum stress of the reinforced PP in the experimental bulk compression test (fully dense cubes), the expected improvement in the mechanical properties of the IWP lattice structure 3D printed using 5 vol% Fe/PP composite filament was not observed clearly during the experimental compression tests.

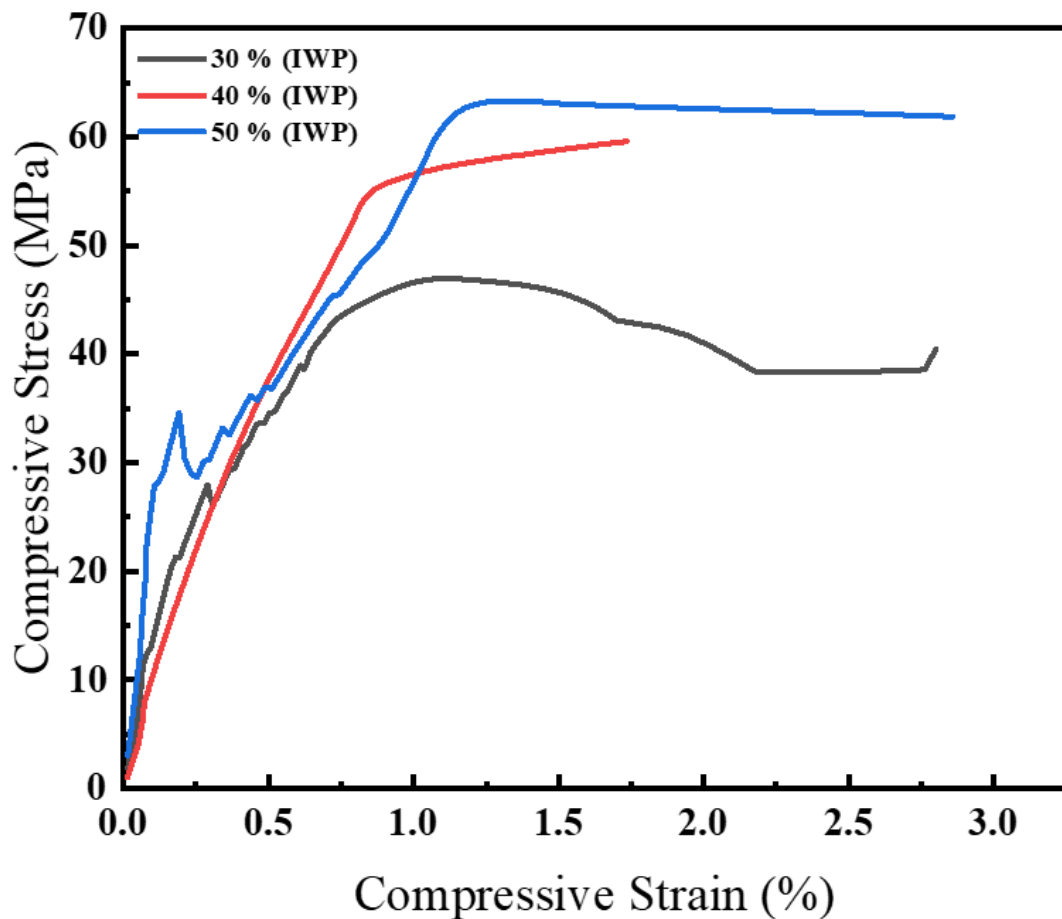


Figure 4.20 Simulated compressive stress-strain graph of 5 vol% Fe/PP IWP.

Figure 4.21 and Figure 4.22 illustrate the finite element analyses depicting the conclusion of the compression test simulations. The color-coded visuals represent the distribution of equivalent stress and the behavior of total deformation. Notably, the stress-strain graphs for IWP specimens with 5 vol% Fe/PP and varying relative densities exhibit consistent patterns in stress and deformation distribution across the samples. The deformation behavior at 3% compressive strain level observed in experiments can be clearly confirmed with the FEA deformation plots. According to Figure 4.21, as a result of the compression test simulations of IWP models, it was observed that the total deformation was concentrated in the upper region of the samples where the force was applied. While the total deformation distribution in the IWP models was not found to be homogeneous, it was observed that the regions characterized by intense and low stress exhibited a homogeneous distribution across the IWP models (Figure 4.22). The consistent distribution of stress throughout the IWP model was indicative of its capability to effectively bear the compressive load. This homogeneity in stress distribution suggests that the structural integrity of the IWP model is well-maintained, with regions experiencing both intense and low stress contributing uniformly to its load-bearing capacity. This observation underscores the model's resilience under compressive forces, highlighting its ability to distribute stress effectively and maintain stability, thereby demonstrating its suitability for applications requiring strength and load-bearing efficiency.

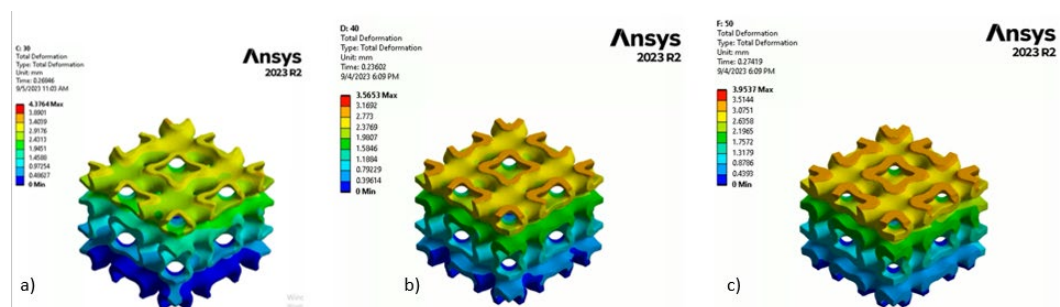


Figure 4.21 Total deformations of compression test modeling of IWP specimens made of 5 vol% Fe/PP composite with (a) 30% relative density, (b) 40% relative density, and (c) 50% relative density.

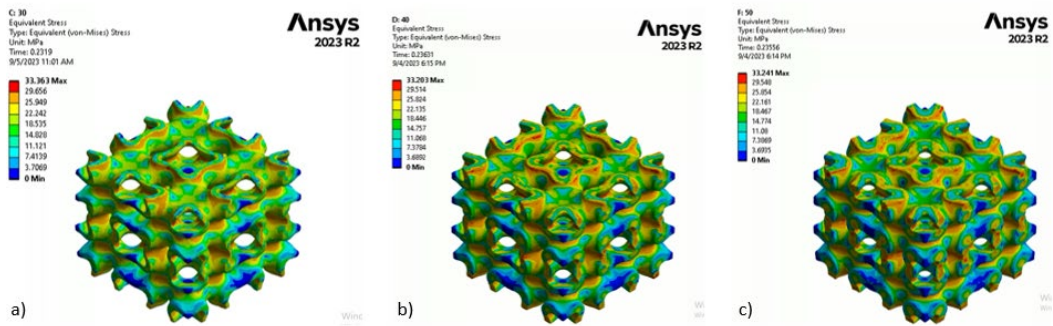


Figure 4.22 Equivalent stress distribution of compression test modeling of IWP specimens made of 5 vol% Fe/PP composite with (a) 30% relative density, (b) 40% relative density, and (c) 50% relative density.

4.4.1 Compression Behavior Comparison between FEM and Experimental Test

Compressive responses of experimentally tested lattices have also been studied by conducting nonlinear static FEA. Figure 4.23 shows the nominal stress-strain curves obtained from compression tests and their corresponding FEA results for pristine PP. According to this graph, simulated (FEM) compressive yield strength of the IWP lattice structure with 40% density made of pristine PP is higher than the experimental compression test result of the same specimens.

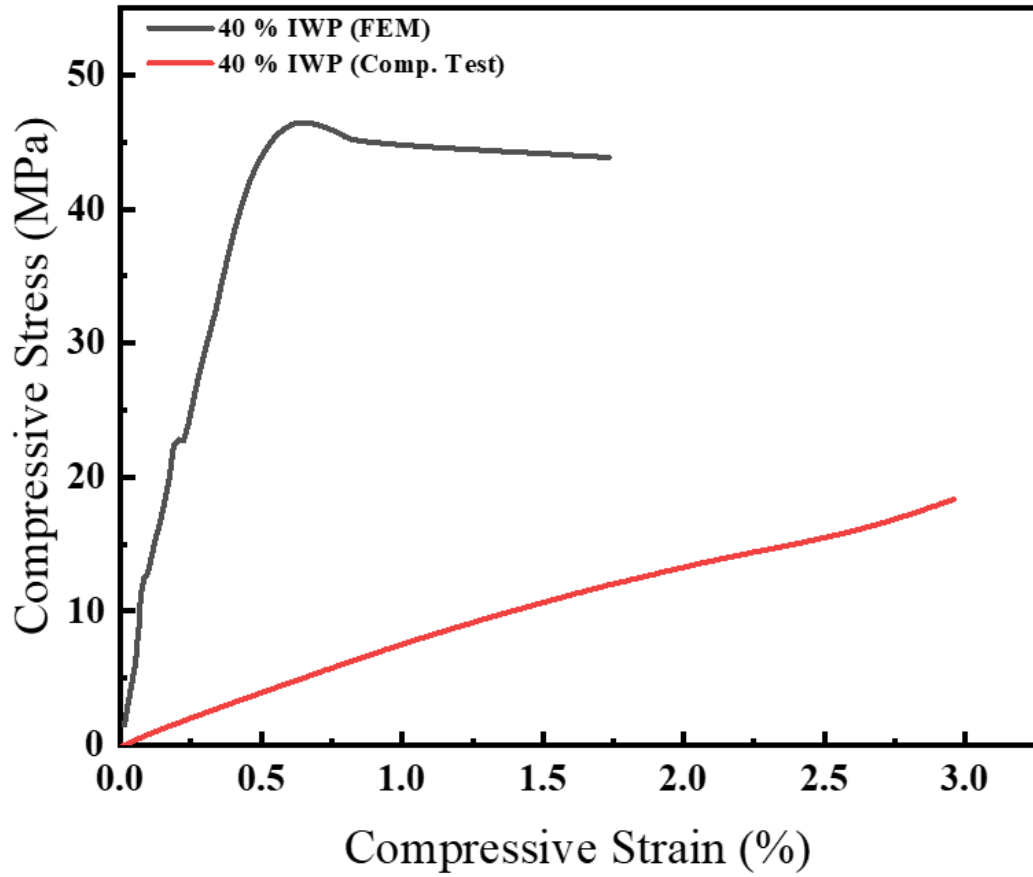


Figure 4.23 Experimentally measured and simulated (FEM) compressive stress-strain curves of the IWP lattice structure with 40% density made of pristine PP.

Graphs in **Hata! Başvuru kaynağı bulunamadı.**4 show the nominal stress-strain curves obtained from compression tests and their corresponding FEA results of IWP models with 3 different densities made of 5 vol% Fe/PP composite filaments. Compared to the experimental compression test results shown in Figure 4.24, simulated compression test results offer significantly higher maximum compressive stress and elastic modulus. Another difference between the experimental compression test and simulation results of the IWP model is that mechanical data trends depend on the relative density of the structure. Both in the experimental and simulated compression test results compressive stress shows a fluctuating trend with compressive strain, yet in general compressive strength seems to be increasing with relative density of the lattice structure.

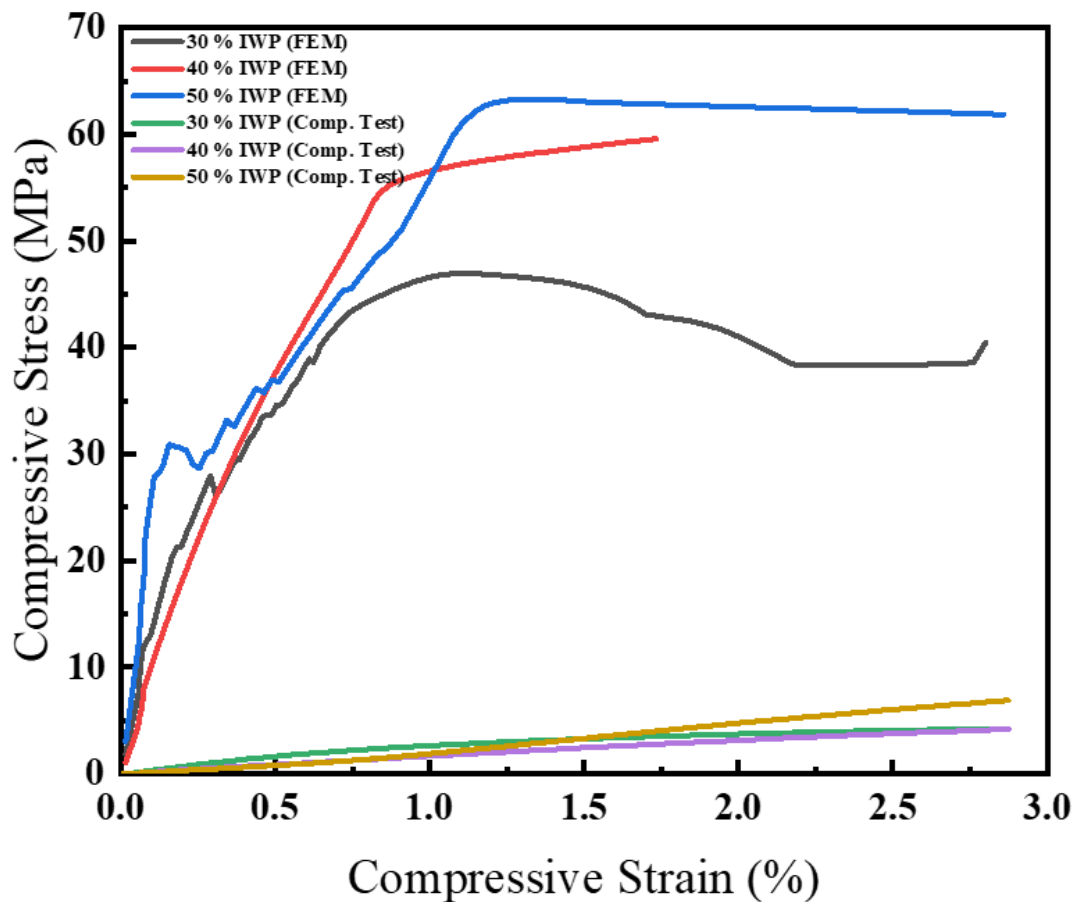


Figure 4.24 Compressive stress-strain curves for comparison of FEM and experimental.

The graphs above (Figure 4.24) indicate no consistency between the finite element models and the experimental results for the compression samples. However, analyses are constrained to the region before the densification due to considerations such as computational time, convergence issues, and absence of dependable data for damage model parameters.

Anticipated disparities between simulated compressive test results and experimental findings were attributed to the inherent limitations of FEM analysis. The expectation was for FEM results to exhibit higher mechanical values due to the inherent assumption of a perfect continuum in the virtual model. However, it is crucial to acknowledge that FEM analyses typically overlook certain additive manufacturing intricacies, such as detachment between layers, the presence of air gaps, voids in the filament, and warping in the fabricated models.

These production discontinuities, inherent in the real-world manufacturing process, introduce variations and imperfections that are not fully captured by the idealized FEM simulations. Consequently, the experimental results tend to reflect the influence of these manufacturing intricacies, leading to observed differences when compared to the theoretically derived FEM results. This recognition underscores the importance of considering real-world manufacturing nuances when interpreting and reconciling the results from computational simulations and physical experiments to enhance the findings' accuracy and applicability.

CHAPTER 5

CONCLUSION

In this study, a detailed examination of the microstructure of metal powder incorporated composite filaments and their use in creating various lattice structures through Fused Filament Fabrication (FFF) has been conducted. The findings and discussions of this study shed light on essential aspects of this specific field, which have several implications for using metal containing filaments in additive manufacturing.

The microstructural analyses revealed that the iron powder used in this study exhibited a plate-like morphology, contrary to the initial expectation of spherical particles due to the gas atomization process. This plate-like morphology could have implications for composite filaments' mechanical behavior and quality, as it may act as a stress concentrator or crack nucleation site. The influence of particle aspect ratio and particle size on the composite filaments' mechanical properties and additive manufacturing (3D printing) quality was discussed. Consideration of these characteristics when designing metal containing filaments for specific applications has been determined to be essential.

The examination of specimens produced by FFF highlighted the importance of even particle distribution and dispersion throughout the filament for a successful 3D printing process. Findings indicated that metal particles containing filaments, especially those with higher metal content, could increase porosity and challenge the adhesion of the printed layers. For lattice structure models (TPMS), it was observed that the high volume percentage of metallic particles can hinder the flow and diameter homogeneity of the composite filament. This can affect the manufacturability of the filament and its suitability for specific 3D printing methods.

Mechanical testing revealed several important insights into the properties of the fabricated structures. Pristine PLA exhibited higher compressive strength than pristine PP, which aligns with the inherent material properties of these polymers. The effect of metal particle incorporation on the mechanical properties was discussed, indicating that while the compressive yield and maximum stress increased with the addition of metal particles in PP matrix fully dense cubes, the same trend was not observed in PLA cubes due to porosity concerns. Moreover, the manufacturability of pristine filaments was generally better than that of composite filaments, especially for lattice structure models.

According to the compression test results of fully dense cubic structures, an improvement in the mechanical properties of metal particle-added PP matrix cubes was detected, depending on the amount of additive. On the other hand, the expected improvement in the mechanical properties of composite structures with added PLA matrix could not be achieved. This situation was associated with the difficulty of manufacturing metal particle containing PLA composite filaments via FFF which also contain air voids.

In the compression test of TPMS structures, among the three models, the results for the pristine PLA and PP models revealed that the IWP structure was more promising. Subsequently, when production was carried out using a composite filament, 30%, 40%, and 50% density versions of the IWP model were produced, while only the 50% density versions of the other models were preferred. Despite some improvement in the mechanical properties of metal added PP matrix structures, no enhancement was observed in PLA matrix structures. This lack of improvement in the mechanical properties of PLA-based TPMS structures was attributed to the low production precision and manufacturability of the composite filaments with the PLA matrix leading to significant detachment problems.

The high standard deviation values in mechanical data point out the fact that these properties are dependent on the manufacturing defect during the additive manufacturing of composite filaments.

The finite element modeling of the IWP structure for uniaxial compression testing revealed differences in mechanical behavior compared to actual testing. Although compression tested metal incorporated PP in the cube form showed improvements in elastic modulus and maximum stress, these improvements were not as pronounced in the IWP structure during compression testing. It was observed that the relative density of the structure played a significant role in the mechanical properties of the lattice models. Further research and optimization may be necessary to fully exploit the potential of metal containing filaments in lattice structure applications.

In conclusion, this study provides a comprehensive understanding of the microstructural characteristics, additive manufacturing quality, and mechanical behavior of metal containing filaments in fused filament fabrication. These findings are crucial for developing and optimizing metal containing filaments for various applications, including lattice structures, where factors such as particle morphology, aspect ratio, and volume fraction can significantly impact the final properties and manufacturability of the filaments. Future research should focus on improving the performance and reliability of metal containing filaments in additive manufacturing processes.

REFERENCES

- [1] Ribeiro, Matos, Jacinto, Salman, Cardeal, Carvalho, Godina, & Peças. (2020). Framework for life cycle sustainability assessment of additive manufacturing. *Sustainability*, 12(3), 929. <https://doi.org/10.3390/su12030929>
- [2] Kruth, J., Wang, X., Laoui, T., & Froyen, L. (2003). Lasers and materials in selective laser sintering. *Assembly Automation*, 23(4), 357-371. <https://doi.org/10.1108/01445150310698652>
- [3] Prashanth, K. G. (2020). Selective laser melting: Materials and applications. *Journal of Manufacturing and Materials Processing*, 4(1), 13. <https://doi.org/10.3390/jmmp40100134>
- [4] Zhang, B., Li, Y., & Bai, Q. (2017). Erratum to: Defect formation mechanisms in selective laser melting: A review. *Chinese Journal of Mechanical Engineering*, 30(6), 1476-1476. <https://doi.org/10.1007/s10033-017-0184-3>
- [5] C. B. Carolo, L., & Cooper O., R. E. (2022). A review of the influence of process variables on the surface roughness of ti-6al-4V by electron beam powder bed fusion. *Additive Manufacturing*, 59, 103103. <https://doi.org/10.1016/j.addma.2022.103103>
- [6] Ziaee, M., & Crane, N. B. (2019). Binder jetting: A review of process, materials, and methods. *Additive Manufacturing*, 28, 781-801. <https://doi.org/10.1016/j.addma.2019.05.031>
- [7] Gibson, I., Rosen, D., & Stucker, B. (2014). *Additive manufacturing technologies: 3D printing, Rapid Prototyping, and direct digital manufacturing*. Springer.
- [8] Wang, F., & Wang, F. (2017). Liquid resins-based additive manufacturing. *Journal of Molecular and Engineering Materials*, 05(02), 1740004. <https://doi.org/10.1142/s2251237317400044>

- [9] Wagner, M. A., Hadian, A., Sebastian, T., Clemens, F., Schweizer, T., Rodriguez-Arbaizar, M., Carreño-Morelli, E., & Spolenak, R. (2022). Fused filament fabrication of stainless steel structures - from binder development to sintered properties. *Additive Manufacturing*, 49, 102472.
- [10] Thompson, Y., Gonzalez-Gutierrez, J., Kukla, C., & Felfer, P. (2019). Fused filament fabrication, debinding, and sintering as a low-cost additive manufacturing method of 316L stainless steel. *Additive Manufacturing*
- [11] Rahman et al. (2015). Mechanical properties of additively manufactured PEEK components using fused filament fabrication.
- [12] Chaturvedi, E., Rajput, N. S., Upadhyaya, S., & Pandey, P. K. (2017). Experimental study and mathematical modeling for extrusion using high-density polyethylene. *Materials Today: Proceedings*, 4(2), 1670-1676. <https://doi.org/10.1016/j.matpr.2017.02.006>
- [13] Dey, A., & Yodo, N. (2019). A systematic survey of FDM process parameter optimization and their influence on part characteristics. *Journal of Manufacturing and Materials Processing*, 3(3), 64. <https://doi.org/10.3390/jmmp3030064>
- [14] Mazzanti, V., Malagutti, L., & Mollica, F. (2019). FDM 3D printing of polymers containing natural fillers: A review of their mechanical properties. *Polymers*, 11(7), 1094. <https://doi.org/10.3390/polym11071094>
- [15] Rodríguez-Panes, A., Claver, J., & Camacho, A. (2018). The influence of manufacturing parameters on the mechanical behavior of PLA and ABS pieces manufactured by FDM: A comparative analysis. *Materials*, 11(8), 1333. <https://doi.org/10.3390/ma11081333>
- [16] Rutkowski, J. V., & Levin, B. C. (1986). Acrylonitrile-butadiene-styrene copolymers (ABS): Pyrolysis and combustion products and their toxicity a review of the literature. *Fire and Materials*, 10(3-4), 93-105. <https://doi.org/10.1002/fam.810100303>

- [17] Lee, J., An, J., & Chua, C. K. (2017). Fundamentals and applications of 3D printing for novel materials. *Applied Materials Today*, 7, 120-133. <https://doi.org/10.1016/j.apmt.2017.02.004>
- [18] Dey, A., Hoffman, D., & Yodo, N. (2019). Optimizing multiple process parameters in fused deposition modeling with particle swarm optimization. *International Journal on Interactive Design and Manufacturing (IJIDeM)*, 14(2), 393-405. <https://doi.org/10.1007/s12008-019-00637-9>
- [19] Dey, A., Hoffman, D., & Yodo, N. (2019). Optimizing multiple process parameters in fused deposition modeling with particle swarm optimization. *International Journal on Interactive Design and Manufacturing (IJIDeM)*, 14(2), 393-405. <https://doi.org/10.1007/s12008-019-00637-9>
- [20] Wang, P., Zou, B., Xiao, H., Ding, S., & Huang, C. (2019). Effects of printing parameters of fused deposition modeling on mechanical properties, surface quality, and microstructure of PEEK. *Journal of Materials Processing Technology*, 271, 62-74. <https://doi.org/10.1016/j.jmatprotec.2019.03.016>
- [21] Padovano, E., Galfione, M., Concialdi, P., Lucco, G., & Badini, C. (2020). Mechanical and thermal behavior of Ultem® 9085 fabricated by fused-deposition modeling. *Applied Sciences*, 10(9), 3170. <https://doi.org/10.3390/app10093170>
- [22] Terekhina, S., Skornyakov, I., Tarasova, T., & Egorov, S. (2019). Effects of the infill density on the mechanical properties of nylon specimens made by filament fused fabrication. *Technologies*, 7(3), 57. <https://doi.org/10.3390/technologies7030057>
- [23] Pakkanen, J., Manfredi, D., Minetola, P., & Iuliano, L. (2017). About the use of recycled or biodegradable filaments for sustainability of 3D printing. *Sustainable Design and Manufacturing 2017*, 776-785. https://doi.org/10.1007/978-3-319-57078-5_73

- [24] Ahn, S., Montero, M., Odell, D., Roundy, S., & Wright, P. K. (2002). Anisotropic material properties of fused deposition modeling ABS. *Rapid Prototyping Journal*, 8(4), 248-257. <https://doi.org/10.1108/13552540210441166>
- [25] Dawoud, M.M.; Saleh, H.M. Introductory Chapter: Background on Composite Materials. In *Characterizations of Some Composite Materials*; InTechOpen: London, UK, 2018.
- [26] Masood, S., & Song, W. (2004). Development of new metal/polymer materials for rapid tooling using fused deposition modeling. *Materials & Design*, 25(7), 587-594. <https://doi.org/10.1016/j.matdes.2004.02.009>
- [27] Kamaal, M., Anas, M., Rastogi, H., Bhardwaj, N., & Rahaman, A. (2020). Effect of FDM process parameters on mechanical properties of 3D-printed carbon fiber–PLA composite. *Progress in Additive Manufacturing*, 6(1), 63-69. <https://doi.org/10.1007/s40964-020-00145-3>
- [28] 89. Li, N.; Li, Y.; Liu, S. Rapid prototyping of continuous carbon fiber reinforced polylactic acid composites by 3D printing. *J. Mater. Process. Technol.* 2016, 238, 218–225. [CrossRef]
- [29] Tao, W., & Leu, M. C. (2016). Design of lattice structure for additive manufacturing. *2016 International Symposium on Flexible Automation (ISFA)*. <https://doi.org/10.1109/isfa.2016.7790182>
- [30] Gibson, L. J. (2005). Biomechanics of cellular solids. *Journal of Biomechanics*, 38(3), 377-399. <https://doi.org/10.1016/j.jbiomech.2004.09.027>
- [31] Schaedler, T. A., Jacobsen, A. J., Torrents, A., Sorensen, A. E., Lian, J., Greer, J. R., Valdevit, L., & Carter, W. B. (2011). Ultralight metallic Microlattices. *Science*, 334(6058), 962-965. <https://doi.org/10.1126/science.1211649>
- [32] AlMahri, S., Santiago, R., Lee, D., Ramos, H., Alabdouli, H., Alteneiji, M., Guan, Z., Cantwell, W., & Alves, M. (2021). Evaluation of the dynamic response of

triply periodic minimal surfaces subjected to high strain-rate compression. *Additive Manufacturing*, 46, 102220. <https://doi.org/10.1016/j.addma.2021.102220>

[33] Mechanical response of a triply periodic minimal surface cellular structures manufactured by selective laser melting

[34] Callister, W. D., & Rethwisch, D. G. (2017). *Materials Science and Engineering: An intro*

[35] Zhang, J., Xie, S., Li, T., Liu, Z., Zheng, S., & Zhou, H. (2023). A study of multi-stage energy absorption characteristics of hybrid sheet TPMS lattices. *Thin-Walled Structures*, 190, 110989. <https://doi.org/10.1016/j.tws.2023.110989>

[36] I. Maskery et al., “Insights into the mechanical properties of several triply periodic minimal surface lattice structures made by polymer additive manufacturing,” *Polymer*, vol. 152, pp. 62–71, Sep. 2018, doi: 10.1016/j.polymer.2017.11.049.

[37] X. Li et al., “Investigation of Compressive and Tensile Behavior of Stainless Steel/Dissolvable Aluminum Bimetallic Composites by Finite Element Modeling and Digital Image Correlation,” *Materials*, vol. 14, no. 13, 2021, doi: 10.3390/ma14133654.